ABSTRACT

Title of dissertation: ATOMIC LAYER DEPOSITION OF
ALUMINUM FLUORIDE FOR USE
IN OPTICAL DEVICES

Alan Uy
Doctor of Philosophy, 2022

Dissertation directed by: Professor Raymond A. Adomaitis
Department of Chemical and Biomolecular Engineering

Thin metal fluoride films are useful as protective and anti-reflection coatings for optical instruments. Aluminum trifluoride (AlF_3), which in the bulk exhibits dielectrical properties of a high band gap (>10 eV) and low refractive index (∼1.35 at 632 nm), makes it an appropriate coating for ultraviolet applications. In this study, AlF_3 atomic layer deposition (ALD) thermochemistry and surface reaction mechanisms between precursors trimethyl aluminum (TMA) and titanium (IV) tetrafluoride (TiF_4), is studied as a means of fabricating these highly conformal films. Based on the hypothesized ALD reaction mechanism, ideal growth per cycle (GPC) is predicted. This work encompasses the design and construction of two ALD reactors for fabricating AlF_3 thin films. A cross-flow reactor design will be shown to successful produce thin films with correct Al to F stoichiometry and refractive index (1.38 at 632 nm). Characterization techniques include X-ray photoelectron spectroscopy (XPS), variable angle spectroscopic ellipsometry, atomic force microscopy (AFM), scanning electron microscopy (SEM) coupled with energy dispersive spectroscopy

(EDS), and spectrophotometry. Because films produced by the cross-flow reactor exhibited film spatial thickness gradients, film impurities, and particle formation, a next-generation showerhead type reactor was designed to reduce precursor flow asymmetries. The simplified design also was subject to fewer sources of leaks and with a modified gas delivery system based on the direct draw of TiF_4 operating at 110°C and TMA operating at room temperature. Self-limiting growth was demonstrated for this ALD process. A collaboration between the University of Maryland and NASA-Goddard Space Flight Center was conducted to overcoat physically vapor deposited Al-LiF mirrors with ALD AlF_3. Detailed reflectivity and maintained performance for these optical mirrors are presented.

ATOMIC LAYER DEPOSITION OF ALUMINUM FLUORIDE FOR USE IN OPTICAL DEVICES

by

Alan Uy

Dissertation submitted to the Faculty of the Graduate School of the
University of Maryland, College Park in partial fulfillment
of the requirements for the degree of
Doctor of Philosophy
2022

Advisory Committee:
Professor Raymond A. Adomaitis, Chair/Advisor
Professor Lourdes Salamanca-Riba
Professor Dongxia Liu
Professor Chen Zhang
Doctor Vivek H. Dwivedi

© Copyright by
Alan Uy
2022

Acknowledgments

I owe my gratitude to all the people who have made this thesis possible. It is difficult for me to put in words how necessary and vital the support I've received throughout this process has been so I'll try to keep it brief.

First and foremost I'd like to thank my advisor, Professor Raymond Adomaitis for giving me an invaluable opportunity to work on challenging and extremely interesting projects over the past years. He has always made himself available for help and advice and there has never been an occasion when I've knocked on his door and he hasn't given me time. It has been a pleasure to work with and learn from such an extraordinary individual.

I must thank Dr. Vivek Dwivedi. He has without a doubt acted as an unofficial co-adviser and has given such strong support for me during all of this work. I have learned so much from you and can only hope to be as good an engineer as you.

I also thank Dr. Manuel Quijada and Dr. Luis Rodriguez de Marcos, and all the other members of the FUV coating team at NASA-Goddard. I am thankful for the opportunity to collaborate on such interesting projects.

I am happy to have had the chance to work with previous and current members of the Adomaitis research group, especially Hossein, Joseph, Aarathi, and Corinne. I also thank my classmates, friends and colleagues in the Chemical and Biomolecular Engineering department. My graduate experience has been one that I will cherish forever.

I would also like to acknowledge help and support from the FABLAB members.

Through this all, I can really only owe my deepest thanks to my family.

I am thankful for the financial support from the NASA supported all the projects discussed herein.

It is impossible to remember all, and I apologize to those I've inadvertently left out – but thank you all and thank God!

Table of Contents

List of Tables

List of Figures

List of Abbreviations

AFM	Atomic Force Microscopy
ALD	Atomic Layer Deposition
ALE	Atomic Layer Epitaxy
CVD	Chemical Vapor Deposition
cpl	close-packed limit
DMAH	dimethylaluminum hydride
EDS	Energy Dispersive X-ray Spectroscopy
FUSE	Far Ultraviolet Spectroscopic Explorer
FUV	Far ultraviolet
GPC	Growth Per Cycle
GSFC	Goddard Space Flight Center
hsd	hard sphere diameter
HST	Hubble Space Telescope
LUVOIR	Large Ultraviolet/Optical/Infrared Surveyor
PCA	Principal Component Analysis
PVD	Physical Vapor Deposition
SEM	Scanning Electron Microscopy
TDMAA	tris(dimethylamido) aluminum)
thd	2,2,6,6-tetramethyl-3,5-heptanedionato
TMA	Trimethylaluminum
VASE	Variable Angle Spectroscopic Ellipsometry
XPS	X-ray Photoelectron Spectroscopy

Chapter 1: Introduction

Nanotechnology has been coined as the development of techniques to understand and control matter within the range of 1 and 100 nanometers.[3] Advances in miniaturization have further expanded this working scale into the Angstrom range (1 x 10^{-10} m), while maintaining highly specific aspect structures. Thin film technology has likewise expanded into this regime and is now a large part of miniaturization techniques. Thin films are synthesized by depositing a layer of solid-state material onto a surface. Development of thin film technology has focused on a multitude of pathways on enhancing the properties of the coating or through the improvement of properties associated with the underlying material. Pathways of improvement for thin films include maintaining or enhancing the uniformity, smoothness, and density of films at scales which can range down to a monolayer, a single layer of atoms or molecules. Such efforts have resulted in the critical development of technologies including optics, LEDs, semiconductor devices, energy storage and conversion, catalysis, and biomedical devices [4, 5, 6, 8].

Techniques for thin film deposition seek to have tunable control on layer thickness as accurate to a single monolayer of the material. Thin film techniques have been divided into two categories: physical and chemical.[10] Most physically based techniques are classified as physical vapor deposition (PVD), which focus on mechanical, electromechanical, or thermal methods to induce vaporization of a material that will deposit onto a targeted surface. For instance, in electron beam physical vapor deposition, an electron beam gun can be used to locally vaporize a small region of a target material while keeping the bulk mostly cool [9]. The vaporization, under high vacuum conditions, then results in gaseous particles having free paths with minimal interactions, directionally depositing onto a targeted surface. As such, it is important to note that this type of directional approach requires that the target material has line-of-sight to the substrate surface. Deposition rates for these processes are, typically measured in nm/s. Other physically based methods include sputtering, molecular beam epitaxy, and thermal evaporation.[10] One example most relevant to this work is the thermal evaporation of aluminum and lithium fluoride for use as a mirror for space optics.[11]

Chemical deposition techniques can be distinguished by the phase of precursor: liquids and vapors fluids [10]. In contrast to physically based techniques, chemical based deposition processes typically focus on using a precursor which reacts with a target surface, resulting in a solid layer. Because of the precursor's fluidity, rather than a line-of-sight path in physically based techniques, all surfaces are exposed to the precursor. As such, the precursor exposure may result in the formation of a thin film on all surfaces within the reactor system. One common example is electroplating, in which a metal coating is generated through the design of an electrolytic cell incorporating a chemical reaction between cathode, anode, and electrolyte. Other chemical methods include chemical solution deposition, sol-gel methods, spin coating, chemical vapor deposition (CVD), and atomic layer deposition (ALD) [15, 16]. This work focuses on exploring the use of ALD as a suitable thin-film deposition technique.

1.1 Atomic Layer Deposition

Prior to 2000, the term atomic layer deposition (ALD) was more commonly referred to as atomic layer epitaxy (ALE) [10]. Historically, the first publications regarding this process were made by Russian scientists in 1969 where the process was described as molecular layering [18]. Early on, the idea of molecular layering did not gain more attention as the layer-by-layer growth from this process was not conducive for generating high yields of product. Gradual interest began with the advent of device miniaturization. In particular, the semiconductor and electronics industry began focusing on generating more densely packed electrical components. This phenomena was observed by Gordon Moose, co-founder of Intel, in 1965 as Moore's Law, an exponential trend postulating that the amount of transistors on a microchip will double roughly every two years. The miniaturization community had renewed interest in ALD as a technique to help satisfy the industrial need for more compact devices. ALD has complimented the continued downscaling of electronic components, as a relatively simple process able to generate high quality thin-films for structures with complex geometries.

Fundamentally, ALD is very similar to CVD, in which vaporized precursors react on a growth surface to generate film.[10, 12] CVD is however different in that its process continuously feeds precursors to the reactor. In contrast, ALD segregates the exposure of vaporized precursors to allow full saturated reaction onto the growth surface, which after exposure to all precursors fulfills the complete ALD cycle. This is conducted by sequentially pulsing each precursor into the reactor resulting in temporally separated precursors or in some cases, segregating exposure by space (spacial atomic layer deposition) [17]. Each precursor adsorbs to the growth surface, resulting in an active surface for the next precursor to adsorb onto.

1.1.1 Atomic Layer Deposition Mechanism

In ALD, volatile precursors are fed to a reactor and react sequentially in a self-limiting fashion onto a growth surface through the cycling of saturating pulses and purges of the precursors. A binary ALD process is illustrated in Figure 1.1:

1. To begin, an important characteristic for an ideal ALD process is that the volatile precursors are stable and do not react in the gas phase; they react only at the growth surface. In the first step of the binary ALD sequence, the first precursor is pulsed into the reactor chamber. Pulses of precursor into a chamber may be performed as a result of direct vapor pressure draw of the precursor or through the use of a carrier gas such as argon or nitrogen to facilitate precursor draw. The gaseous precursor makes contact to the growth surface and undergoes an absorption reaction onto an active surface site through physical or chemical mechanisms. The activation energy barrier for this reaction is activated through thermal energy in thermal ALD. The

dosage time for the precursor is sized such that the reactants are allowed to fully interact with the finite number of active surface sites.

2. The second step of this process, now having a saturated surface, also has unreacted precursor molecules as well as any reaction gaseous by-products formed remaining in the gaseous phase. An inert gas is used to flush the reactor from all reactive gaseous species. The purge time for this segment is designed long enough such that the reaction by-products and unreacted precursors resulting from the first step are sufficiently exhausted from the chamber. Thus, the surface is prevented from any further interaction from the first precursor.
3. In similar fashion to the first step, the third step now pulses the secondary precursor. This precursor reacts and adsorbs to the previous surface, resulting in a new growth surface. The pulse time again is set such that the secondary precursor has sufficient time to interact and fully saturate the substrate surface.
4. The last step of the ALD cycle is a final purge of byproducts and residual excess precursors.

By repetition of this dose-purge-dose-purge cycle, the resulting film thickness grown will depend on the number of cycles performed. ALD film growth is described in terms of growth per cycle (GPC) rather than a growth rate as a steady function of time. Due to all potential physical and chemical interactions, detailed reaction

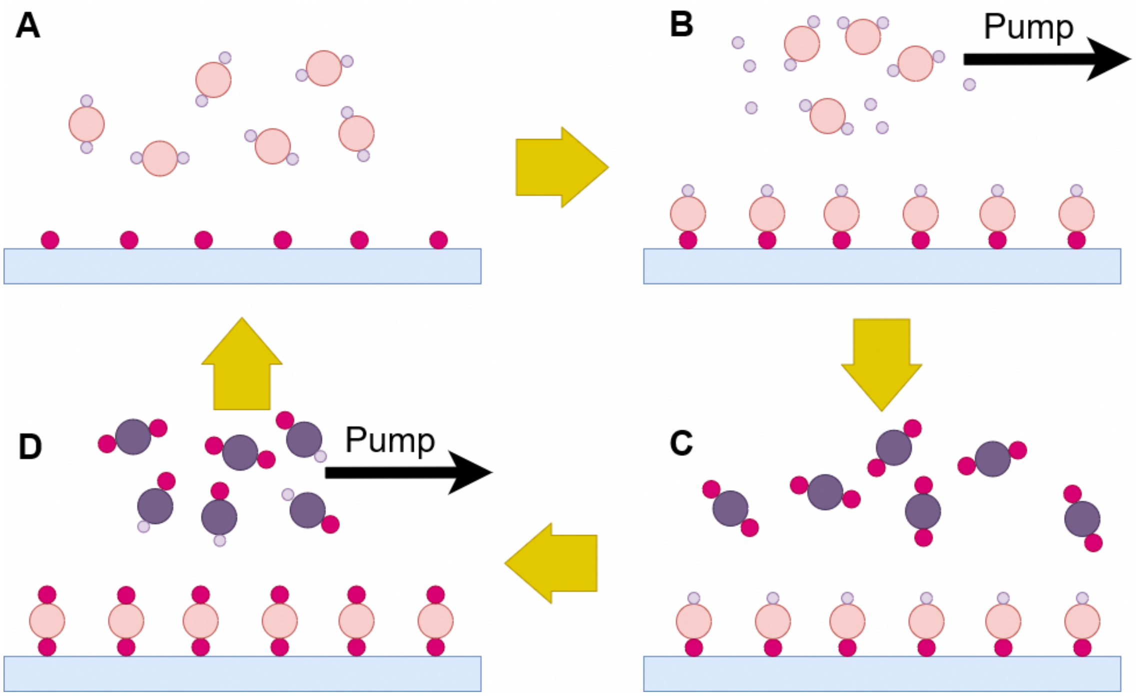

Figure 1.1: General schematic for a typical ALD cycle in four steps featuring two precursor dosages (A,C) and two purges (B,D). Repetition of these steps results in an overall deposition of a thin-film thickness dependent on the amount of cycles performed.

mechanisms and GPC for an ALD process depend largely on the precursors used. Hundreds of ALD binary precursor systems have been identified through research to generate a wide range of thin films: oxides, metals, nitrides, sulfides, and much more.[19] Research in new ALD processes is expanding, resulting in newly discovered precursor systems and ALD mechanisms.[20]

1.2 Motivation

The main motivation for this work is related to space optics technology through enhanced mirror coatings. One of the latest NASA missions, Large UV/Optical/IR Surveyor (LUVOIR), seeks to operate in a very broad spectral region, including the far ultraviolet (FUV) spectrum.[25] There is strong interest in a subset of the far ultraviolet range called the Lyman range (90-120 nm), which is said to be one of the richest bandpasses for astronomy [22]. Exoplanet biospheres in range of habitable zones of host stars undergo photo-dissociation for molecules H_2O and CO_2 and produce bio-signatures of O_2 and O_3[21]. By scanning for the exoplanetary adsorption of H I Lyman-α (91.2 - 121.6 nm), O I (98.9 nm), and C II (103.7 nm), exoplanet atmospheres can be characterized and a high resolution planetary mapping of surrounding planetary systems can be formed.[21, 25] Molecular hydrogen is the most abundant molecule in the universe yet due to its electronic ground-state transition lying below 115 nm, can be difficult to measure as photon emissions are absorbed within Earth's atmosphere, thus requiring measurement in space [24]. Other ion and neutral emissions at higher wavelengths have been considered for mapping, however are more likely to be complicated by other sources such as reflected solar continuum, resulting in a lower resolution map [25]. The previous NASA mission involving the Far Ultraviolet Spectroscopic Explorer (FUSE) had made great strides at mapping at this FUV region, however noted a decline in image resolution stemming from degraded reflectivity of lithium fluoride coated Al mirrors in the FUV range and was attributed to LiF's hygroscopicity and moisture.[23]

Thin metal fluoride films have been considered extensively for spacecraft application as a passivating coating for optics. A thin transparent coating of a metal fluoride such as magnesium fluoride (MgF_2) and lithium fluoride (LiF) has in the past been applied onto pure aluminum mirrors in famous space telescopes such as the Hubble Space Telescope (HST) and Far Ultraviolet Spectroscopic Explorer

(FUSE).[21] Pure aluminum is said to have one of the highest intrinsic reflectances over a broad spectral range; other mirror materials such as gold and silver show great reflectance in visible range however drop heavily in the UV range [23]. The main challenge with working with pure aluminum mirrors is that contamination reactions with oxygen and water spontaneously form aluminum oxide. While the aluminum will eventually passivate itself with a thin layer of aluminum oxide, the oxide layer causes a considerable narrowing of the operable spectral range specifically in the ultraviolet range.[30] Passivating optical coatings must have other properties of low refractive index and low roughness for telescope optics as multiple mirrors within an instrument can compound bending and scattering effects to highly reduce throughput to receiver.[23] As such, the main objective for metal fluoride coatings on aluminum mirrors is to passivate and protect the surface of mirror from oxide formation while having a minimal impact on the underlying mirrors optical properties.

1.2.1 Aluminum Fluoride

A thin film optical coating material currently being investigated is aluminum trifluoride (AlF_3), which in the bulk exhibits dielectrical properties of a high band gap (>10 eV) and low refractive index (∼1.35 at 632nm).[26, 28] Optically, a high band gap can be advantageous, as it helps to ensure low interaction at energetic wavelengths. For thin films that are transparent, this is important as this leads to lesser absorption for wavelengths extending into the more energetic far ultraviolet range. A low refractive index close to n = 1 and absorptance coefficient k close to 0, helps to ensure low bending and dispersion of incoming waves. For a transparent thin film, these properties can help to ensure a minimal impact for potentially sensitive optical applications such as lasers and mirrors. AlF_3 has multiple reported crystalline structures of which all form a three-dimensional network of corner-sharing AlF_6 octahedra, with the only thermodynamically stable phase being α-AlF_3.[4] Other applications for AlF_3 thin films include battery cathode interfaces, lithography, as well as in heterogeneous catalysis.[4, 5, 6, 27, 29, 36] Thin films of AlF_3 have been grown with a variety of methods, such as the physical vapor deposition-based methods of sputtering, electron beam deposition, and ion assisted deposition, and in more recent years, through chemical vapor deposition and atomic layer deposition (ALD) [5, 7, 9, 27, 28, 29, 48].

Aluminum fluoride is currently prospective to operate in the UV range as a material less hygroscopic than LiF and greater transmission spectral range than MgF_2.[22] The exact detail by which hygroscopicity affects LiF is not reported, but an assessment can be made of aluminum fluoride's overall stability regarding atmospheric effect using thermophysical properties. The Gibbs free energy of atmospheric reaction can be calculated using data provided by NIST webbook regarding enthalpies and entropies of formation and summarized in Table 1.1.[50] Atomic oxygen and water are considered for reaction with aluminum fluoride in the following two equations:

$$AlF_3 + H_2O \rightarrow 6HF + Al_2O_3 \qquad \text{(I)}$$

	$\Delta_f H^\circ_{gas}$	$S^\circ_{gas,1bar}$	$\Delta_f G^\circ_{gas}$
AlFO (g)	-581580	237.3	-652331
AlF_3 (s)	-1510420	66.48	-1530241
H_2O (g)	-241830	188.84	-298133
HF (g)	-272550	173.78	-324363
Al_2O_3 (s)	-1675690	50.92	-1690872
O (g)	249180	161.059	201160.3
F_2 (g)	0	202.8	0

Table 1.1: Compiled thermophysical properties of various oxides, fluorides, and others in J/mol ($\Delta_f H^\circ_{gas}$, $\Delta_f G^\circ_{gas}$) and J/mol-k ($S^\circ_{gas,1bar}$) at standard conditions (NIST Chemistry WebBook)[50]

$$AlF_3 + O \rightarrow AlFO + F_2 \qquad \text{(II)}$$

Atomic oxygen is of interest for conditions in low earth orbit, 180-650 km above Earth [49]. In this region, the sun's ultraviolet portion photodissociates diatomic oxygen, where due to low atmospheric density, is unable to recombine into ozone and remains as atomic oxygen. Thermodynamical calculations of reactions (I) and (II) at standard temperature and pressure conditions show an overall positive Gibbs energy of reaction, 313 kJ/mol (I) and 676 kJ/mol (II). This indicates an unlikely reaction involving incorporation of oxygen in the overall bulk film, intuitive as fluorine is much more electronegative than oxygen. On the other hand, assessment of overall reaction between pure aluminum and water reaction into aluminum oxide and hydrogen is heavily favorable (-796.4 kJ/mol), confirming the spontaneity of oxide formation for bare aluminum.

Aluminum fluoride is currently being investigated as a way to enhance optics as performing yet resilient transparent thin coatings. With the prospective nature of AlF_3 thin films, the overall motivation of this work is to investigate the quality of film grown through ALD designed using two novel precursors, trimethyl aluminum and titanium tetrafluoride. While both precursors have been seen in previous ALD studies, use of the precursors together for ALD has not been established. Furthermore, reaction mechanisms using TiF_4 as a precursor for ALD is not well documented. The proposed work hopes to achieve answers towards the following questions:

- Will this ALD precursor system react to form AlF_3?
- Is this process viable for ALD, i.e. are films able to be generated linearly with respect to thickness and cycles, and reproducibly under self-limiting growth?
- How do we qualify the quality of the film and will it be suitable for spacecraft application?

Answers to these questions will have multiple broad impacts: 1) Formalized ALD study for this particular precursor system 2) Established reactor design suitable for solid low vapor pressure precursors that may extend to other potential inorganic chemistries 3) Possible extension for generating conformal coatings on materials requiring complex topographies.

1.3 Outline of Dissertation

In this dissertation, I describe a new novel ALD precursor system using trimethyl aluminum and titanium tetrafluoride with design of two reactor systems for depositing aluminum fluoride thin films. In Chapter 2, we summarize current ALD precursor systems for aluminum fluoride and propose an ALD reaction pathway for generating AlF_3 thin films and predict growth per cycle. In Chapter 3, we discuss the initial development of AlF_3 ALD design and process using a flow-type design reactor. In Chapter 4, we investigate the tunable parameters of ALD process on AlF_3 self-limiting growth using a showerhead type reactor. In Chapter 5, we discuss the AlF_3 thin film application for space optical devices.

Chapter 2: Investigation of precursor systems for aluminum fluoride ALD

2.1 Introduction

Precursor choice is key to the successful design of an ALD process. Aluminum fluoride film generation through a binary ALD process must be designed with two precursors, one to provide the aluminum and the other fluorine. Other desired properties for ALD precursors are that they have sufficient vapor pressure to overcome conductance limitations in the gas delivery system and reactor back pressure, high thermal stability, and high reactivity towards the active surface sites.[32] A number of published ALD precursor systems related to the study of thin films of AlF_3 has been compiled in Table 2.1.

As a source of aluminum, trimethyl aluminum (TMA) has widely been used in ALD processes and is a gold standard for ALD precursors due to its well-documented properties of volatility, thermal robustness, and chemical reactivity towards both substrate surface and secondary precursors.[31] $AlCl_3$, dimethylaluminum hydride (DMAH), and tris(dimethylamido) aluminum (TDMAA) also have been studied for

ALD Study	Thin Film	Metal Precursor	Oxidizing Precursor	T_{range} (°C)
Mäntymäki et al.[5]	AlF_3	$AlCl_3$	TiF_4	160-340
Lee et al.[29]	AlF_3	TMA	HF	75-300
Hennessey et al.[48]	AlF_3	TMA	HF	100-200
Jackson et al.[36]	AlF_3	TMA	TaF_5	125-200
Vos et al.[9]	AlF_3	TMA	SF_6 (plasma)	50-300
DuMont et al.[37]	AlF_3	TMA	HF	155-245
Messina et al.[34]	AlF_3	TMA	HF (plasma)	100
Hennessey et al.[33]	AlF_3	DMAH	HF	150-300
	AlF_3	TDMAA	HF	150-300
	AlF_3	TMA	HF	150-300
Pilvi et al.[35]	MgF_2	$Mg(thd)_2$	TiF_4	225-450
	CaF_2	$Ca(thd)_2$	TiF_4	225-450
	LaF_3	$La(thd)_3$	TiF_4	225-450
Pore et al.[38]	TiO_2	TiF_4	H_2O	300-500

Table 2.1: Published precursor systems related to the study of AlF_3 ALD with reported deposition temperature range (thd = 2,2,6,6-tetramethyl-3,5-heptanedionato, DMAH = dimethylaluminum hydride, and TDMAA = tris(dimethylamido) aluminum).

AlF_3 film generation.[5, 33] It has been noted that when designing ALD precursor systems for use in space optics, where purity of film (absence of O/N) is critical for optical performance, it can be beneficial to avoid certain organometallics that include O and N in their composition.[34]

As the secondary precursor, ALD precursors that provide the source of fluorine are not as common in ALD studies compared to precursors providing oxygen and nitrogen.[35] One of the main challenges in working with fluorine precursors is that the ALD processes can generate acidic products such as hydrogen fluoride (HF) which is undesirable as these byproducts may etch the deposition surface, damage reactor equipment over time, and potentially contribute to the transport and incorporation of etched contaminants onto the growing film.[5, 29] Using HF directly as a precursor requires specialized handling of this corrosive gas and reactor system components resistant to HF etching.

Alternative benign fluoride precursors have been investigated for use in ALD. The use of SF_6 has been demonstrated in plasma-enhanced ALD as a non-toxic gaseous halogenated precursor.[9] However, SF_6 requires an additional, non-thermal means of increasing reactivity, which may reduce the ability to coat nonplanar geometries. Halogenated metal solid-state precursors, such as TiF_4 and TaF_5 have also been studied as potential HF alternatives.[5, 35, 36, 38] TiF_4 and TaF_5 have demonstrated suitable reactivity and thermal stability for ALD as moderate vapor pressure solids precursors. Furthermore, the use of metal fluorides facilitates safe handling as HF is not generated as a byproduct, and products can be readily condensed and separated from process exhaust gases.[35] We do note that a metal-halogen precursor used as the source of the non-metal film component is generally uncommon in ALD.

2.1.1 Titanium tetrafluoride vapor pressure

TiF_4 exist in the solid phase as polymer chains with a Ti coordination of six, and in the gas phase is coordinated as four.[51] A previous report by Hall et al. (1957) had developed an empirical model for TiF_4 vapor pressure as the following[52]:

$$\log_{10} P_{atm} = -5331.51/T - 2.567 \log_{10} T + 16.631, \quad \text{(T in K)} \tag{2.1}$$

With this in mind, prior to ALD study, a preliminary vapor pressure study with TiF_4 (98%) precursor sourced from Strem Chemicals was conducted. A Fomblin pump (Edwards RV5F) was used to first reduce measured line pressure of a connected pressure transducer (Infinicon CDG100) and closed TiF_4 precursor vessel to 1E-3 Torr. A valve was then closed between pump and pressure transducer, maintaining vacuum. The precursor sublimator was then opened to the line and heated between 25°C and 140°C using a controllable MKS heater jacket and transducer readings were recorded. Measured vapor pressure of sublimated gas is summarized in Fig. 2.1, showing good agreement to the empirical formula. Moreover, a suitable vapor pressure from this precursor for ALD study was confirmed starting at 110°C at 0.15 Torr.

2.2 Proposed ALD reaction mechanism

In atomic layer deposition, the reaction mechanism for a binary precursor ALD system is typically represented as two half-reactions, one for each precursor. There is importance in developing the ALD reaction mechanism as it can help explain anomalous growth modes[31]. In the case of aluminum fluoride, the overall reaction between trimethyl aluminum and titanium tetrafluoride to deposit solid $AlF_3(s)$ hat maximizes precursor conversion is:

$$4\mathrm{Al(CH_3)_3(g)} + 3\mathrm{TiF_4(g)} \rightarrow 4\mathrm{AlF_3(s)} + 3\mathrm{Ti(CH_3)_4(g)} \tag{2.2}$$

For describing the ALD half reactions occuring during sequential pulsing, we

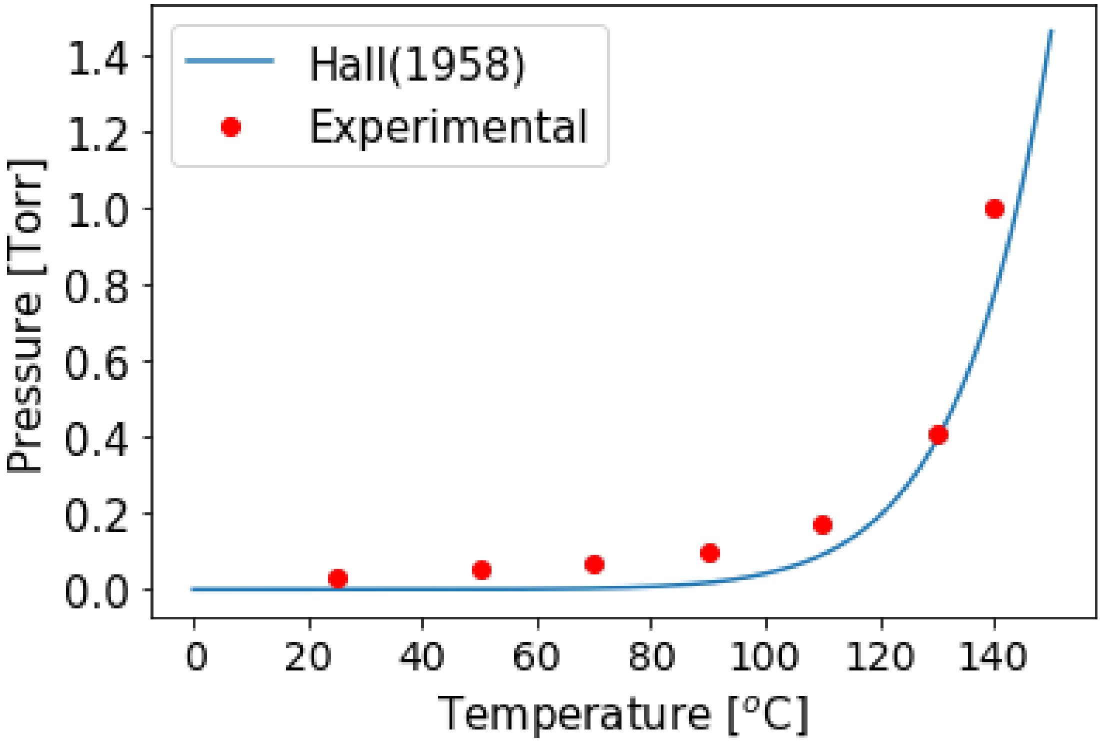

Figure 2.1: In-line vapor pressure of TiF_4 precursor (98%) sourced from Strem Chemicals, measured from between 25°C-140°C and compared to empirical curve by Hall et al. (1958).

note the importance of gas (g), substrate surface (s), and bulk film (b). While there is an initial transitional growth onto the substrate, the proposed reaction mechanism focuses on bulk film growth of AlF_3 and thus is assumed to react with a fluorinated surface. Solid AlF_3 has an octahedral crystalline form with Al^{3+} at the octahedron center and six F^- at the vertices resulting in a F-terminated film surface. With F^-(s) acting as Lewis-base surface sites, TMA(g) adsorbs onto the surface F^-(s) forming the Lewis acid-base adduct. From TMA and water reaction studies, TMA adsorbed TMA half reaction during the TMA exposure period is expected to form dative bonds with substrate surface and physisorb in the following manner:[31, 46]

$$\mathrm{Al(CH_3)_3)(g) + F^{-1}(s) \rightarrow F^{-1}(b){:}Al(CH_3)_3(s)} \tag{2.3}$$

Thus, after a saturating TMA exposure, with Al directing adsorption onto surface, the substrate surface is covered by close-packed ligands of terminal methyl groups.

TiF_4 is less well-known as an ALD precursor and its reactions with the growth surface are not as well-established for ALD. In the reported study of $AlCl_3$ and TiF_4 it was proposed that a ligand exchange mechanism between Cl and F occurs during TiF_4 exposure to aluminum chlorine lined surface.[5, 39] We postulate that, during TiF_4 exposure, due to the octahedral configuration and the four highly electronegative fluorines, the Ti center exhibits Lewis acid behavior. Similarly, due to the bulk film, aluminum having six coordination number, the aluminum at the surface should experience local Lewis acidity. In this Lewis acid-base manner, the TiF_4 gas is theorized to form a dative bond with a surface CH_3 while Al forms a dative bond with F as a metastable complex before proceeding with an irreversible ligand transfer reaction:

$$\mathrm{Al(CH_3)_3(s) + TiF_4(g) \rightleftharpoons TiF_4{:}Al(CH_3)_3^{\ddagger}(s)} \tag{2.4}$$

$$\mathrm{TiF_4{:}Al(CH_3)_3^{\ddagger}(s) \rightarrow AlF(CH_3)_2(s) + TiF_3CH_3(g)} \tag{2.5}$$

Exposure to saturating TiF_4 doses subsequently form dative bonds with the remaining surface methyl groups to promote further ligand exchange reactions in the following manner:

$$\mathrm{TiF_4{:}AlF(CH_3)_2^{\ddagger}(s) \rightarrow AlF_2CH_3(s) + TiF_3CH_3(g)} \tag{2.6}$$

$$\mathrm{TiF_4{:}AlF_2CH_3^{\ddagger}(s) \rightarrow AlF_3(s) + TiF_3CH_3(g)} \tag{2.7}$$

Thus, after a saturating TiF_4 exposure, the surface is now terminated with fluorine bound to aluminum.

The initial thermodynamic analysis for this deposition mechanism appears favorable for depositing AlF_3. The overall deposition reaction described by (2.2) is unusual compared to more common ALD processes (e.g., alumina ALD using TMA and H_2O) and $Ti(CH_3)_4$ thermochemical data is less readily available. However, if we consider the bond dissociation energies listed in Table 2.2, the ligand exchange reaction:

$$\text{Al-CH}_3 + \text{Ti-F} \rightarrow \text{Al-F} + \text{Ti-CH}_3 \tag{2.8}$$

Bond	Δ H^o, kJ mol^{-1}	
Al–C	255	
Al–F	664	$\Longrightarrow \Delta\text{H} = -409$ kJ mol^{-1}
Ti–F	569	
Ti–C	435	$\Longrightarrow \Delta\text{H} = 134$ kJ mol^{-1}

Table 2.2: Bond energies relevant to the proposed ligand exchange reactions taken from [40] indicating the net exothermic ΔH that results when F replaces C bonded to Al, and the considerably smaller endothermic ΔH for the replacement of F with C bonded to Ti.

is exothermic with a net ΔH_{rxn} of -275 kJ mol^{-1} and appears to be potentially favorable for generating aluminum fluoride bonds assuming relatively small entropy change.

2.3 Thin film growth model

It is important to distinguish the terms growth per cycle (GPC) and growth rate when characterizing thin film deposition process. Growth rate in thin film depositions is described by rate units of nm/s or Å/s, but ALD's layer by layer growth is generally measured in Å/cycle of thin-film addition. ALD studies most often use GPC to describe the amount of material deposited during each ALD cycle. Some ALD studies use "growth rate" and GPC interchangeably; GPC in Å/cycle will only be used in this thesis.

2.3.1 ALD surface state

Based on the proposed reaction mechanism, we now consider the problem of describing the instantaneous state of the surface over the complete cycle. For our ALD reaction mechanism, we denote the surface species of aluminum (Al) and fluorine (F) resulting after each ALD half-cycle and also note methyl groups (Me) which are bound to Al. Following the notation of Travis et al. (2013), we denote brackets [ ] for surface species number densities and hat (̂) as the theoretical maximum.[41] Through this, we define a ligand coverage ratio value $\theta_X = [\mathrm{X}]/[\hat{\mathrm{X}}]$ for species X.

To compute the maximum surface concentrations, we define a molecular number density relation $\rho_{AlF_3} = \rho N_A / m_{AlF_3}$, of which $\rho = 2.9$ g/cm^3 is AlF$_3$ film density, N_A is Avogadro's number, and m$_{AlF_3}$ = 83.98 g/mol is the molecular mass of AlF$_3$.[29, 50] From this we find $\rho_{AlF_3} = 20.79$ nm^{-3}, which is interpreted as the effective volume occupied by a single molecule of AlF$_3$. An ideal monolayer thickness (Δ_z) then can be calculated as $\Delta_z = \sqrt[3]{1/\rho_{AlF_3}}$, and is found to be 3.64 Å.

For the consideration of an ALD film generated from a cycling between the TMA and TiF$_4$ precursors, we consider the resulting growth surface after a saturating TMA exposure, resulting in a surface covered by methyl groups. Following Travis et. al (2013), $[\hat{\mathrm{Me}}]$ is approximated by the Me hard sphere diameter and the close packing limit. The ideal close packing limit of cpl$_{Me} = \pi\sqrt{3}/6 \approx 0.9069$, a value calculated by Friedrich Gauss through geometrical arguments as the highest fraction of space that can be occupied by discs in 2D. For Me, the hard sphere diameter value is hsd$_{Me}$ = 4.010 Å, a value found by simulation using Lennard-Jones parameters for CH$_3$ radicals[44], this closely matches to the Van der Waals radius of 2 Å used by Puurunen(2003).[42] With these values, the surface depicted by Figure 2.2 features a 2D slice of close-packed methyl groups. This gives the maximum

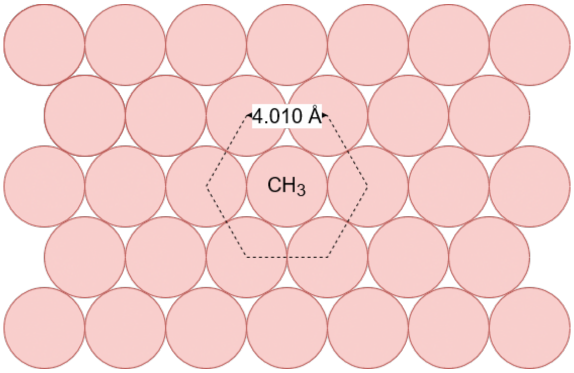

Figure 2.2: Growth surface saturated with the maximum number density of CH_3 ligands after a saturating TMA exposure

surface number density $[\hat{\mathrm{Me}}]$ over an area A = 1 nm^2:

$$[\mathrm{Me}] = \frac{cpl_{Me} * A}{(\pi(hsd_{Me}/2)^2)} = 7.18\mathrm{Me/nm}^2, \tag{2.9}$$

a value found to be in agreement with Travis. This results in $\hat{[}\mathrm{Al}] = [\hat{\mathrm{Me}}]/3 = 2.39$ Al atoms per nm^2. This gives the ligand exchange ratio as $\theta_{AlF_3} = [\mathrm{AlF}_3]/[\mathrm{A\hat{l}F}_3] = 0.3166$ and our GPC can be calculated as:

$$\mathrm{GPC} = \theta_{Al}\Delta_z = 1.15\text{Å}/\mathrm{cycle} \tag{2.10}$$

As is obseved in many other ALD processes, even under ideal saturating conditions, this process is limited to approximately 1/3 monolayer GPC.

As a further refinement to the model, rather than performing the calculation with the dense packing of methyl ligands, a model based on the predicted radius of the TMA molecule is proposed. We assume TMA with planar configuration with the three CH_3 ligands assembled in a flat, triangular arrangement. With r_L as the Van der Waal's radius of CH_3 we approximate the hard "disk" radius of planar adsorbed

TMA by geometry:

$$r_{TMA} = \frac{r_L}{\cos(\pi/6)} + r_L \tag{2.11}$$

with Van der Waals radii of 2 Å used by Puurunen(2003), the hard disk radius is calculated to be $r_{TMA} = 0.43$ nm. We assume these hard "disks" to randomly pack the surface whereby the close random packed limit disk density on a 2-dimensional surface of $\phi_{rcp} = 0.8525$ was recently calculated.[43]. The calculation for the adsorbed TMA surface density [$\hat{\text{TMA}}$] follows as:

$$[\hat{\text{TMA}}] = \frac{\Phi_{rcp} A}{\pi r_{TMA}^2} = 1.46\ \text{TMA/nm}^2. \tag{2.12}$$

During TiF_4 exposure, we again assume complete ligand exchange of F for CH_3 ligands and the fraction f of monolayer Δ_z deposited each cycle and ALD GPC is predicted:

$$f = \frac{[\hat{\text{TMA}}]\Delta_z^2}{A} = 0.194 \tag{2.13}$$

$$\text{GPC} = f\Delta_z = 0.705\ \text{Å/cycle}. \tag{2.14}$$

The refined GPC calculation is hypothesized to act as the upper limit for expected GPC from ALD reactor system.

2.4 Final Remarks

In this chapter, previous ALD precursor systems pertaining to aluminum fluoride was reviewed. TMA and TiF_4 have been established suitable for ALD study but has never been used together for film deposition. While HF precursor in AlF_3 deposition has been used extensively in previous studies, TiF_4 was chosen for this study as a prospective alternative ALD precursor able to avoid HF formation and thus TiF_4 vapor pressure was studied. An ALD reaction mechanism for TMA and TiF_4 half-cycles is proposed by which adsorption of precursors and a ligand-exchange during TiF_4 half-cycle ultimately generate AlF_3. Further discussion of additional potential reactions and detailing of reaction mechanisms is presented in subsequent chapters. The 2D surface random packing limit of TMA adsorbed molecules was used to describe the ALD surface state during saturating pulses, and GPC of ALD AlF_3 growth using TMA and TiF_4 was predicted to be 0.705 Å/cycle.

Chapter 3: Process development for atomic layer deposition of aluminum fluoride

3.1 Introduction

There are several basic requirements for ALD reactor design. First, the reactor must be able to heat substrates to a controlled deposition temperature. Second, controlled pulses of precursors must be injected into the reactor body while inert gas is used to purge reaction byproducts and excess reactants. Meanwhile a vacuum pump is used to continuously pump the reactor to reach a certain pressure, which can be from sub-Torrs to atmospheric pressure pressure.[12] As ALD is not a continuous process, the reactor volume is constantly filled and purged in cycles, requiring automation to control reactant and inert gas solenoid valves as well as exhaust gate valves.

There are several classified types of ALD reactor configurations that are used across in industry and academia.[12] As a high-level classification, ALD reactors are typically split between flow-type and showerhead designs.[13] In flow-type reactors, feed gases flow parallel over the substrate before exhausting out of reactor body through the pump, which depending on flow input and pumping speed may be laminar or turbulent. In showerhead reactors, gas flow impinges perpendicularly onto the substrate often through a perforated or porous flow diffuser to help distribute inlet gases evenly before exhausting out through the pump. ALD reactors also are classified by the method to control deposition temperature as either hot-wall or cold-wall.[10] In hot-wall reactors, the substrate equilibriates with the temperature of the reactor body walls whereas in cold-wall reactors, the reactor body may remain cool while a sample stage heater heats the substrate. Additional care to ensure thermal equality throughout reactor in hot-wall reactors may be necessary if ALD growth is sensitive to temperature, otherwise gradients may occur.[14] In cold-wall reactors, care must be given to prevent condensation of precursors on walls as this may result in unintended reactions that can influence growth or introduce impurities into the film. Lastly, a carrier gas (often the same composition as the purge gas) may be used to help deliver precursors to the substrate. In the absence of a carrier gas, direct draw of a precursor with sufficient vapor pressure also has been used in ALD systems.

For industrial scale applications of ALD, large batch reactors may be used to coat multiple wafers in one run; however, the larger volume of reactor may increase precursor and byproduct mass transfer limitations, potentially lengthening cycle times from requiring longer dose and purge times. Spatial ALD reactors can reduce processing time for large scale applications. Rather than separating pulses and purges by time intervals, spatial ALD substrates instead positionally move between fixed precursor inlet zones in which exposure to different precursors simultaneously occur within the reactor.[17]

In this chapter, we describe the development of a laboratory scale ALD reactor for AlF_3 coatings using a TMA and TiF_4 precursor system in a flow-type reactor. A nominal ALD recipe consisting of precursor flow and purge timing sequences was designed. Deposited films were characterized using scanning electron microscopy (SEM) with energy dispersive X-ray spectroscopy (EDS), X-ray photoelectron spectroscopy (XPS), and variable-angle spectroscopic ellipsometry. Film properties and growth rate were found to be dictated by TiF_4 dosage. Higher-dosed samples resulted in surprisingly high growth, but with high refractive indexes and significant Ti, O, and C incorporation. Lower-dosed samples were found to have a growth per cycle (GPC) of under 0.5 Å with refractive indices at 632 nm wavelength as low as 1.34 and little O and C incorporation. Additional reaction mechanisms representing the underlying surface chemistry observed for this ALD system are presented and used to investigated how process operating conditions affect growth rate and film contamination.

3.2 Materials and methods

This study uses a custom-built hot-wall laminar flow-type reactor; a schematic of the reactor is illustrated in Figure 3.1. The main body of the reactor is outfitted with a controllable gate valve which connects to two Mass-Vac filters (Visi-Trap with

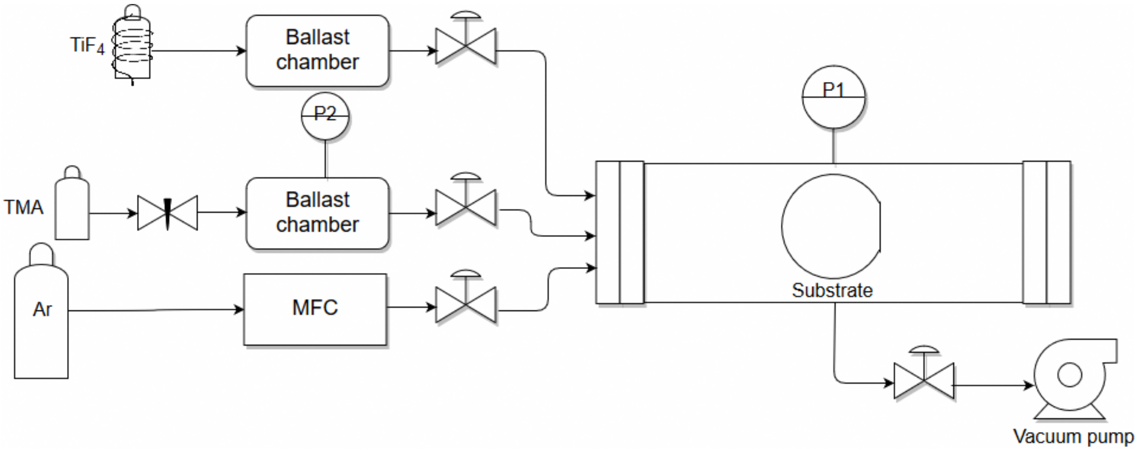

Figure 3.1: Schematic design of experimental ALD reactor laminar flow-type flow

SodaSorb and Posi-Trap with activated charcoal) before an Edwards model RV5F mechanical vacuum pump which ultimately exhausts into a fume hood. MKS ALD pneumatic valves control precursor flow from the precursor bubbler (TMA) and sublimator (TiF_4) through a multi-input flange on the reactor body. Purge gas feed is controlled with a mass flow controller (MKS P-series). A heating line is wrapped around the main reactor body and is controlled with PID temperature controllers that operate within a range of 100-200°C. Capacitance manometers are connected to the TMA precursor line (Infinicon AG Li-9496) and reactor main body (Baratron 624D) for monitoring pressures; during nominal operation the reactor chamber base pressure measures ∼0.1 Torr. An illustration of the reactor is seen in Figure 3.2.

The substrates consist of single side polished Si(100) 2-inch wafers with ∼1.5 nm native oxide layer purchased from Virginia Semiconductor. The TiF_4 (98%) was supplied from Strem Chemicals and TMA (97%) from Aldrich Chemistry. Ultra-high purity grade argon (99.999%) is used as purge gas and was supplied from Airgas. The TiF_4 sublimator is wrapped with a separate heating line and is controlled with

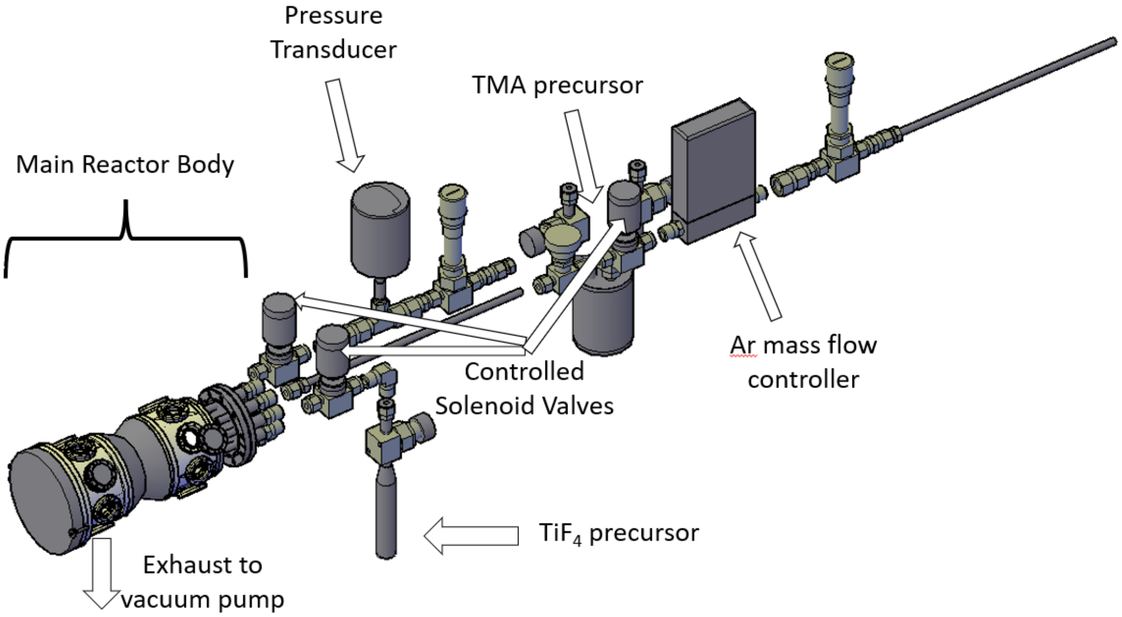

Figure 3.2: Graphical illustration of experimental ALD reactor laminar flow-type flow, an additional pressure transducer (not shown) is attached to a view port in the reactor main body.

a separate PID controller to operate within a temperature range between 50-160°C while TMA was maintained at room temperature. Wafers were solvent cleansed with ethanol in an ultrasonic bath for 5 minutes, rinsed with deionized water, and dried prior to deposition.

ALD recipe design for the reactor system is defined by a combination of set operating conditions and timing sequences. The controllable operating conditions consist of reactor deposition temperature T_{rxr} and TiF_4 precursor temperature T_{TiF_4} for this reactor design. Pulse, purge, and exposure time sequence for each precursor is defined for a cycle; the recipe repeats the timings for a specified number of ALD cycles. As such, a nominal timing sequence for our binary precursor system is denoted t_1-t_2-t_3-t_4. For our system, t_1 refers to pulse time of TMA, t_2 purge time for reactor following the first pulse, t_3 the pulse time of TiF_4, and t_4 the subsequent purge time associated with TiF_4, all in seconds. When higher precursor doses were desired, the reactor exhaust gate valve was shut after t_1 and t_3 for specified lengths of time.

All measurements of samples were conducted ex-situ. Optical measurements for thickness and refractive index were conducted using a J. A. Woollam M-2000D variable angle spectroscopic ellipsometer (VASE) at the University of Maryland NanoCenter at 65° and 70° angle settings. Film optical characterizations were generated using J. A. Woollam CompleteEASE software. Thickness and refractive index maps were generated by measuring 19 points in hexagonal patterns about the wafer center. Elemental composition was characterized with a Kratos AXIS 165 X-ray photoelectron spectrometer (XPS) at the University of Maryland Surface Analysis Center. Binding energies were calibrated with carbon (284.80 eV) with take off angles of 20° and 90°. A Hitachi SU-70 scanning electron microscope (SEM) with energy dispersive spectroscopy (EDS) also was used to characterize film composition.

3.3 Initial experimentation

For this study, we initially considered multiple sets of process recipes for depositing AlF_3 films. Confirmation of film growth with this new precursor system was accomplished using our process recipe consisting of 200 cycles of a simple four pulse-purge timing sequence of 0.1s-30s-0.1s-30s with a reactor temperature setpoint of 100°C and TiF_4 precursor source heated to 70°C. However, significant amounts of loose particles were generated with this process. Origin of the particles was later confirmed to be as artifacts of TiF_4 direct draw and were to be mitigated by incorporating a 7 micron in-line mesh filter between the TiF_4 precursor and reactor chamber. For this otherwise successful first run, mean film thickness was measured to be 27 nm through ellipsometry. XPS analysis showed a 1:3.08 Al:F atomic % ratio with contaminants of Ti, O, and C totaling nearly 10 at.% after surface cleaning by sputtering.

A range of recipes specifying precursor pulse and purge times, reactor temperature, and total number of cycles were tested to assess the effect on film GPC and composition. Thickness maps are presented for a subset of six films (A-F) compiled through J. A. Woollam CompleteEASE software in Fig.3.3. In general, it was consistently observed that the maximum thickness corresponded to the wafer point closest to the reactor TiF_4 inlet in the 2 o'clock position. Directional gradients along precursor have also been reported in other AlF_3 ALD systems.[5, 9]

We examined the growth per cycle (GPC) for the subset of runs [A, B, C] whose recipe differed only by the total number of cycles. Process parameters for the [A, B, C] subset is summarized in Tab. 3.1. Films in this set of runs were produced using a timing sequence of 0.1-30-0.1-30 s, reactor temperature of 180°C, and TiF_4 source temperature of 120°C. The mean GPC was found to be [0.31, 0.25, 0.16 Å] for [200, 400, 700] cycles, respectively. In comparison $AlCl_3$-TiF_4 and TMA-HF-pyridine ALD systems have reported GPC values of 1.7 Å at 200°C and 0.74 Å at 175°C, respectively.[5, 29] Film thickness data for runs [A, B, C] versus cycles are plotted in Fig. 3. Mean thickness appears to plateau with increasing cycle number while the maximum thickness suggests the more linear growth expected for an ideal ALD

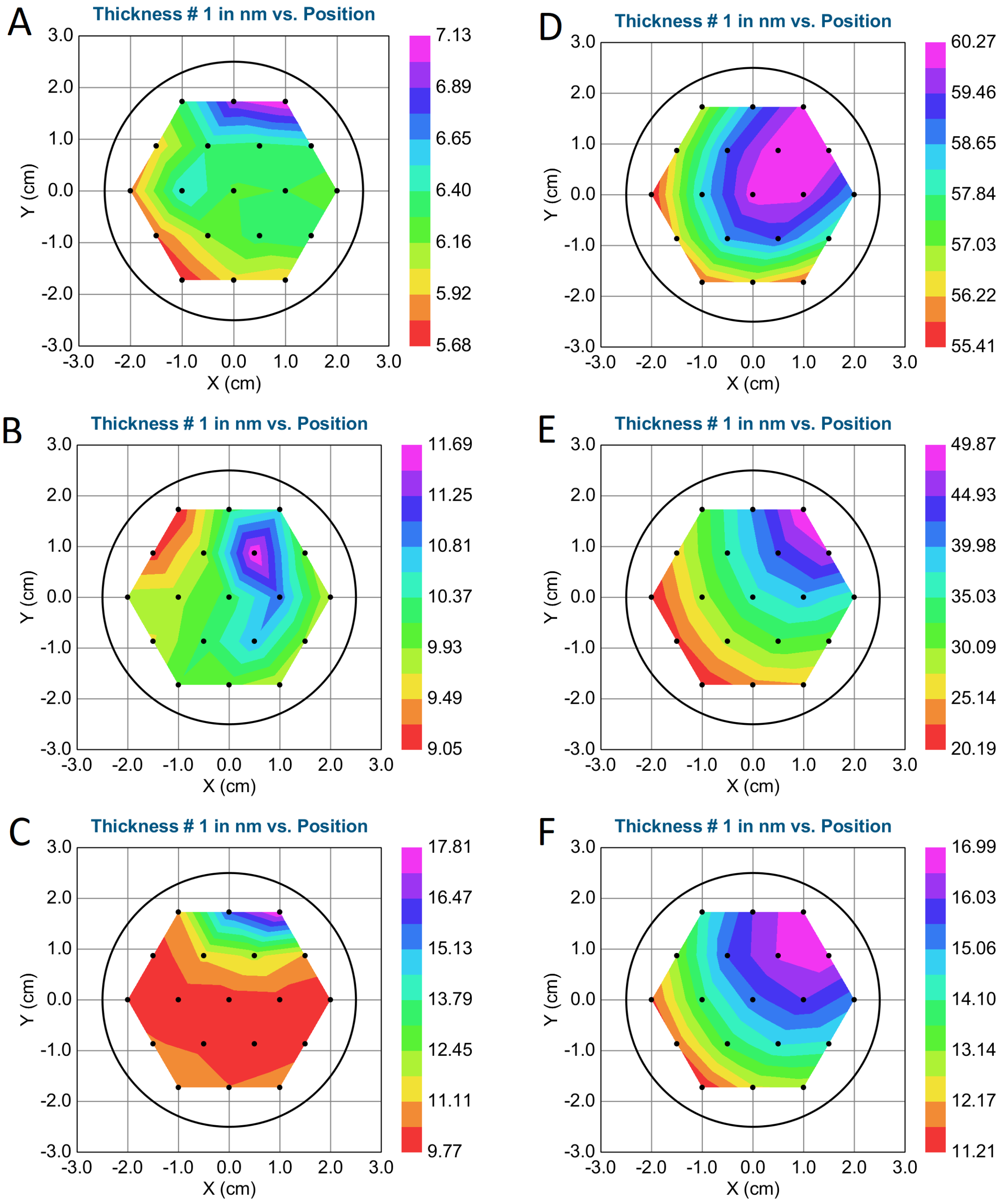

Figure 3.3: Contour maps of the AlF3 thickness across a 2" Si wafer as determined from spectroscopic ellipsometry mapping regarding samples A through F. The thickness gradient towards the bottom-left correlates with the positional entry of TiF$_4$ precursor from the top right. TMA precursor enters from the top left.

Sample	Timing sequence (s)	ALD cycles	T$_{rxr}$ (°C)	T$_{TiF_4}$ (°C)
A	0.1-30-0.1-30	200	180	120
B	0.1-30-0.1-30	400	180	120
C	0.1-30-0.1-30	700	180	120
D	0.1-30-1-4-30	100	190	140
E	0.1-60-1-4-60	150	190	140
F	0.1-120-1-4-120	100	190	140

Table 3.1: Summarized process parameters for experiments A through F.

process. Vos et al. (2017) has reported a thickness range of 19.8-23.3 nm across wafer, which matches the observed maximum-minimum thickness encountered in samples A and B, but not sample C. The 700 cycle sample [C] showed significant widening of maximum to mininum disparity of 8 nm as opposed to ranges of 1.5 nm and 2.6 nm for samples [A] and [B], respectively. Thus, these observations suggests an insufficient exposure of the wafer surface to TiF_4 past 400 cycles despite having increased precursor source temperature since our initial run (from 70°C to 120°C for runs [A, B, C]). From this, we hypothesized that partial clogging of the TiF_4 delivery system (particularly, the in-line filter as it often required cleaning between runs) over the course of longer runs is the source of decreasing doses with increasing number of total cycles.

The next subset of experiments [D, E, F] examined film qualities under TiF_4 saturating conditions. To ensure a fully saturating dose of TiF_4, these films were grown using a higher deposition temperature and TiF_4 precursor temperature setting: $T_{TiF_4} = 140°C$, $T_{rxr} = 190°C$, as well as a modified timing sequence of 0.1-x-1-4-x, in which x refers to length of purge after precursor dose. Process parameters for the [D, E, F] subset is summarized in Tab. 3.1. Samples D, E, and F use purge time

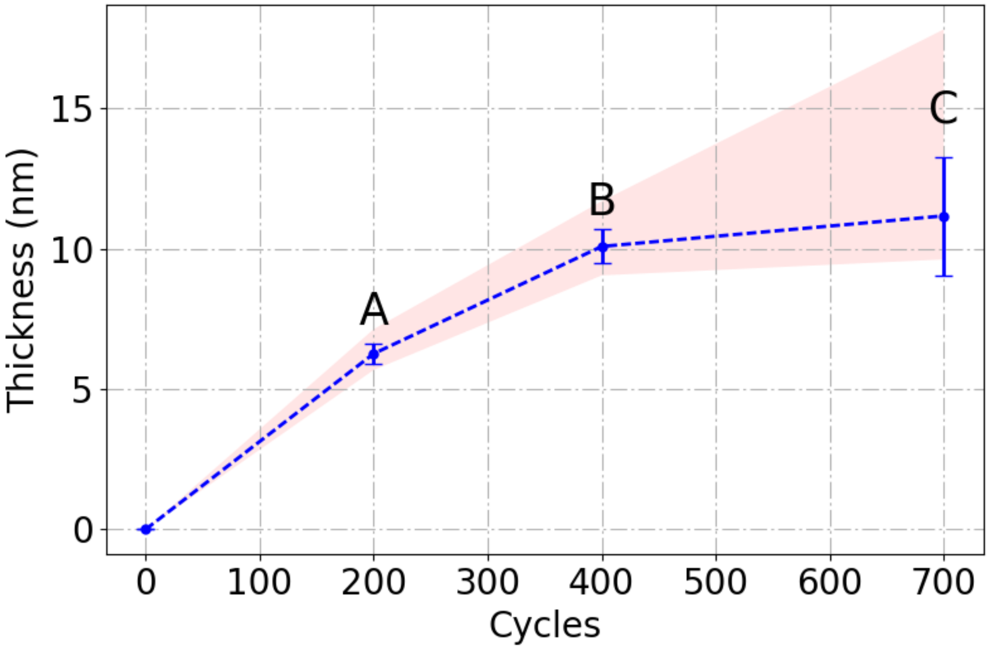

Figure 3.4: Thickness vs ALD cycles data generated for runs A, B, and C. Blue data points represent average thickness of wafer with error bars of 1 standard deviation. Highlighted area represents thickness range measured over the wafer.

lengths x_D, x_E, and x_F of 30, 60, and 120 secs, respectively. The fourth number in timing sequence refers to 4 seconds of time after the TiF_4 pulse in which the gate valve to the pump is closed to ensure saturation. The resulting GPC is plotted as a function of purge length in Fig. 3.5, where 100 cycles were completed in runs D and F while 150 cycle were completed in E. While run D has the same length of purge as experiments [A, B, C], the film produced in D grew at maximum 6 Å/cyc versus the maximum of 0.31 Å/cyc from the previous [A, B, and C] set. Additional tests altering purge times for TMA did not affect GPC while lengthened post-TiF_4 purge times showed a trend of decreased GPC. Runs conducted using these high doses of TiF_4 were found to never exceed 6 Å/cyc. Interestingly, this growth rate is about double that of the calculated ideal monolayer for crystalline AlF_3. Additionally, the inverse dependence of GPC on purge time found in Fig. 3.5 indicates a mode in which adsorbed TiF_4 may desorb from surface to decrease growth rate, which is later discussed in Section 3.4.1.

3.3.1 Film Composition

Film composition was assessed through XPS analysis for runs B, D, E, and F without sputtering of surface. XPS spectra for the four runs are summarized in Fig. 3.6. All samples showed signatures of Al, F, O, and C; however samples corresponding to high doses of TiF_4 [D, E, F] indicated additional signals of Ti. As seen in Fig. 3.6, sample B does not appear to show a significant Ti peak; CasaXPS peak fitting found Ti content to be negligible. With respect to longer purge lengths,

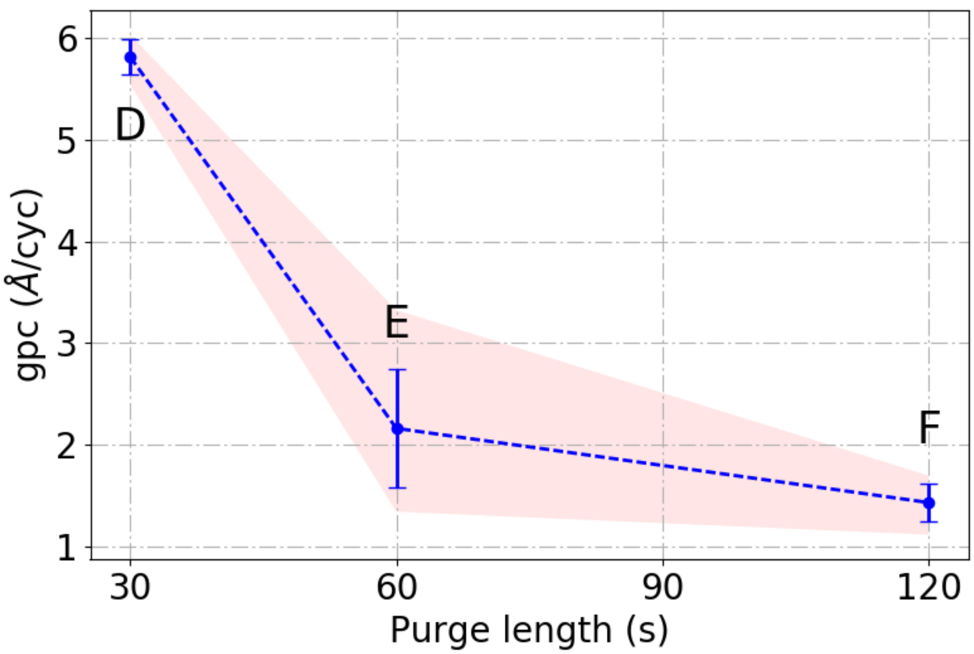

Figure 3.5: Runs D, E, and F are summarized by GPC (Å) vs purge length for high-dosage TiF_4 runs. Blue data points represent average thickness on wafer with error bar of 1 standard deviation. Highlighted area represents the gpc range measured over the wafer.

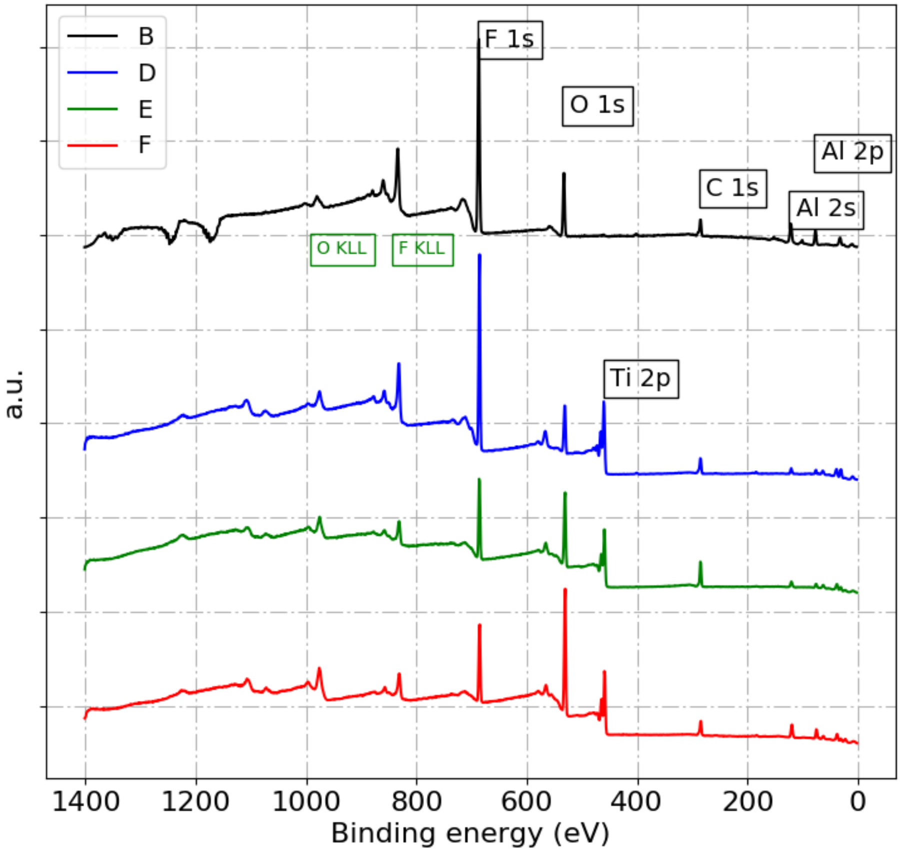

Figure 3.6: XPS spectra corresponding to a full 0-1400 eV scan on AlF_3 samples featuring low (B) and high doses (D, E, and F) of the TiF_4 precursor.

it was found that the binding energy for O grows in signal relative to F. Film composition in atomic % was calculated for the four runs using CasaXPS software and the results are compiled in Table 3.3.1.

Analysis of the high resolution scans are summarized in Fig. 3.7. Run B features a binding energy peak at 76.6 eV. Although slightly shifted from crystalline α-AlF_3 (77.1 eV), this value nonetheless matches Al 2p binding energy found from other ALD studies AlF_3 film.[5, 48, 53] Runs D, E, and F show major peaks found between reference AlF_3 and Al_2O_3 signals, which are likely to indicate AlO_xF_y.[45, 54]

20° takeoff

Sample	B	D	E	F
C	23.5	49.1	56.5	36.7
O	19.7	19.5	24.6	32.8
Al	17.9	10.2	7.2	15.7
F	38.9	16.7	7.4	9.8
Ti	0	4.5	4.2	4.9

90° takeoff

Sample	B	D	E	F
C	15.3	18.3	29.7	16.3
O	17.6	17.5	29.3	40.2
Al	20.4	9.2	9.9	16.9
F	46.6	44.8	22.7	18.7
Ti	0	10.2	8.5	7.8

Table 3.2: XPS results for atomic % composition using two takeoff angles for the 400 cycle ALD sample B and the saturating TiF_4 samples D, E, and F.

In addition to AlO_xF_y, a secondary peak is found near 71 eV possibly indicative of an Al-Ti alloy.[50, 55] In Fig. 3.7 (b), a binding energy peak at 687 eV is found for run B, matching closely with other F 1s signals found from ALD prepared AlF_3.[5, 48] In contrast, runs D, E, and F show binding energy peaks which shift heavily towards the TiF_4 reference signal (684.9 eV) indicating significant TiF_4 incorporation.[56] A slight shift of the F 1s signal towards AlF_3 can be observed from Fig. 3.7 (b) when using longer purge times.

Carbon and oxygen contaminants are expected to appear due to film exposure to laboratory air on removal from the reactor. Evidence of adventitious carbon is seen on the carbon 1s spectra, in which any carbon was found primarily bonded to itself or to oxygen. The compositional analysis summarized in Table 3.3.1 also showed high C in the 20° takeoff data relative to 90° suggesting C to be located more primarily in the surface, whereas the other elements remained more consistent between the two measurements. In the oxygen 1s spectrum of Fig. 3.7 (d), binding energy values are seen ranging between metal oxides and carboxides. Oxygen-carbon bonds are seen represented in the O 1s spectra as expected, yet for runs D, E, and F, peaks shift towards metallic oxides associated with aluminum and titanium. Thus, for run B, oxygen primarily exists with adventitious carbon, whereas runs D, E, and F have oxygen embedded within a metal-halide structure.

Titanium incorporation in metal fluoride films when using TiF_4 as an ALD precursor has been found to decrease by increasing deposition temperature.[5, 35] Similarly, high Ta incorporation was observed when TaF_5 precursor was used as the fluorine source.[36] Unexpectedly high growth rates of AlF_3 have been thought to be due to excess adsorption of TiF_4 leading to additional growth reactions during each ALD half reaction as opposed to the initial proposed reaction mechanism.[5] These past observations are consistent with the high GPC found in runs D, E, and F. Yet, when considering film composition as a function of purge time length, it is interesting to note the relative increase of oxygen together with a decrease of titanium and fluorine. It is expected that longer purge times (e.g., run F) enhance surface titanium fluoride precursor desorption, affecting the aluminum-to-titanium ratio. Evidence for this is seen as the binding peak shifts toward AlF_3 in the F 1s spectra for run F. Meanwhile, run F also showed a large increase of oxygen atomic % relative to the other elements. O incorporation is feasible as TiF_4 and water has been used to form TiO_2 under ALD conditions.[38]

The high O content found in the XPS results is undesired for this ALD process. From Table 3.3.1, sample D had the shortest purge time and exhibited a higher relative amount of F:O as well as Ti atomic %, suggesting a low rate of TiF_4 conversion. As another potential source of oxygen in film, DFT studies have suggested enhanced interaction of water to undercoordinated aluminum near the surface.[45] High surface-area structures of AlF_3 are said to become extremely Lewis acidic and

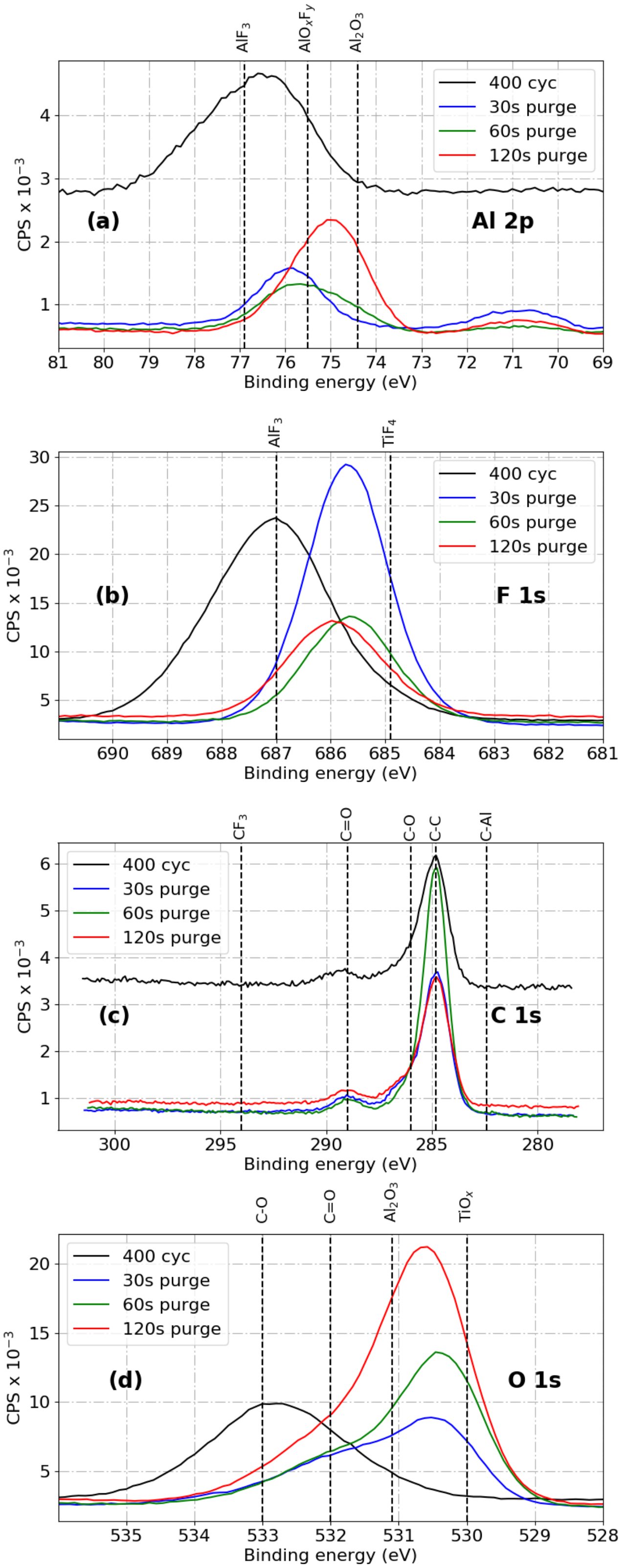

Figure 3.7: High resolution spectrum scans about peaks associated with Al 2p (a), F 1s (b), C 1s (c), and O 1s (d) states. Reference signals are taken from literature[5, 48, 53, 56] and NIST Chemistry webbook.[50]

will react with ambient water and stabilize as AlFO.[4] It is possible that the longer purge times of E and F resulted in such a structure that allowed access into the bulk film to react with ambient water vapor upon removal of the deposited film from the hot reactor chamber.

3.3.2 Optical Properties

AlF_3 absorbs light in the far UV (below wavelengths of 200 nm). However, samples prepared by ALD have shown some absorption below 4.1 eV (wavelengths <300 nm).[9, 26] For this study, a Cauchy model was used to characterize film properties at wavelengths between 300-1000 nm using the CompleteEASE software. The characterization used three constant parameters to fit for thickness and refractive index with the following Cauchy dispersion formula[47]:

$$n(\lambda) = A + \frac{B \times 10^4}{\lambda^2} + \frac{C \times 10^9}{\lambda^4}, \quad (\lambda \text{ in nm}) \tag{3.1}$$

Runs A, B, and C were found to have averaged refractive indices (632.8 nm wavelength) and standard deviations $n = [1.46 \pm 0.04, 1.470 \pm 0.02, 1.34 \pm 0.04]$, respectively. The higher-dosed TiF_4 samples [D, E, F] had higher refractive indices of $n = [1.49 \pm 0.002, 1.87 \pm 0.03, 1.86 \pm 0.04]$, respectively. Mäntymaki et al. reported a refractive index for semicrystalline AlF_3 to be 1.36 and so our higher refractive indices are attributed to the incorporation of contaminants in the film.[5] For runs E and F, which had a high O:F ratio, the refractive index increased to values between that of ALD-grown amorphous alumina ($n = 1.60$ at 177 °C) and

ALD-grown amorphous TiO_2 ($n = 2.34$ at 150 °C).[57, 58]

A reassessment of film optical properties for a subset of samples was conducted after one year. Run C showed little change in refractive index after one year. Interestingly, the average overall refractive index decreased by 3% with several wafer points measuring ±0.05 from previously measured values. Variance in measured points is expected to be due to slight placement differences between wafer measurement locations between the original measurements and those taken one year later. Five other samples were remeasured to find an average refractive index decrease of 1.1%.

3.4 Deposition reaction mechanism

Examining deposition reaction pathways for ALD systems gives insight into film growth behavior through GPC and potential routes to impurity incorporation.

3.4.1 Excess TiF_4 adsorption

As described earlier, the GPC of experiments A, B, and C all are less than the previously calculated ideal ALD GPC = 0.7 Å/cycle predicted by our analysis; we conclude that insufficient TiF_4 precursor was supplied to the reactor in these runs resulting in incomplete conversion in the second half-reaction. This behavior is in contrast to runs D, E, and F which all resulted in much higher GPC than anticipated as observed in Fig. 3.5.

To understand the higher than ideal GPC of runs D, E, and F, we consider the reaction mechanism of Mäntymäki, and coworkers[5] who proposed a "double-layer" growth mode model to account for GPC values higher than that which would be found under the ideal ALD cycle described earlier (note that the precursor system used in their study was TiF_4 and $AlCl_3$). In the solid state, TiF_4 molecules are known to bind strongly in a polymeric form.[51] This opens the possibility of additional adsorption of TiF_4 on the growth surface during the second half-cycle after the CH_4, F ligand exchange reactions are complete. Using our estimate of the hard-sphere diameter of TiF_4:[1]

1. We propose that n layers of TiF_4(g) adsorb onto the AlF_3 surface resulting in the adsorption of $n \times [\hat{TiF_4}] = n \times 3.07$ adsorbed TiF_4 per nm^2 where $n \geq 0$.
2. During the subsequent TMA half cycle, the additional n TiF_4(a) layers results in an additional $n \times (4/3)$ AlF_3 nm^{-2} added to the overall film growth
3. before the final, saturating layer of TMA adsorbs to repopulate the surface to $[T\hat{M}A] = 2.01$ TMA nm^{-2}.

Under this excess-adsorption mechanism, we find that

$$\text{GPC} = \Delta_z^3 \left([T\hat{M}A] + n \times \frac{4}{3} [T\hat{i}F_4] \right). \tag{3.2}$$

As seen in Fig. 3.8, the resulting GPC model (3.2) predictions are consistent with the high GPC values found for experimental runs D, E, and F corresponding to TiF_4 over-saturation. In this figure, we note that $n = 0$ corresponds to ideal ALD

---

[1] Due to lack of data for the TiF_4 hard-sphere diameter, we use the known value for CCl_4 of 590×10^{-12} m as an approximation[60].

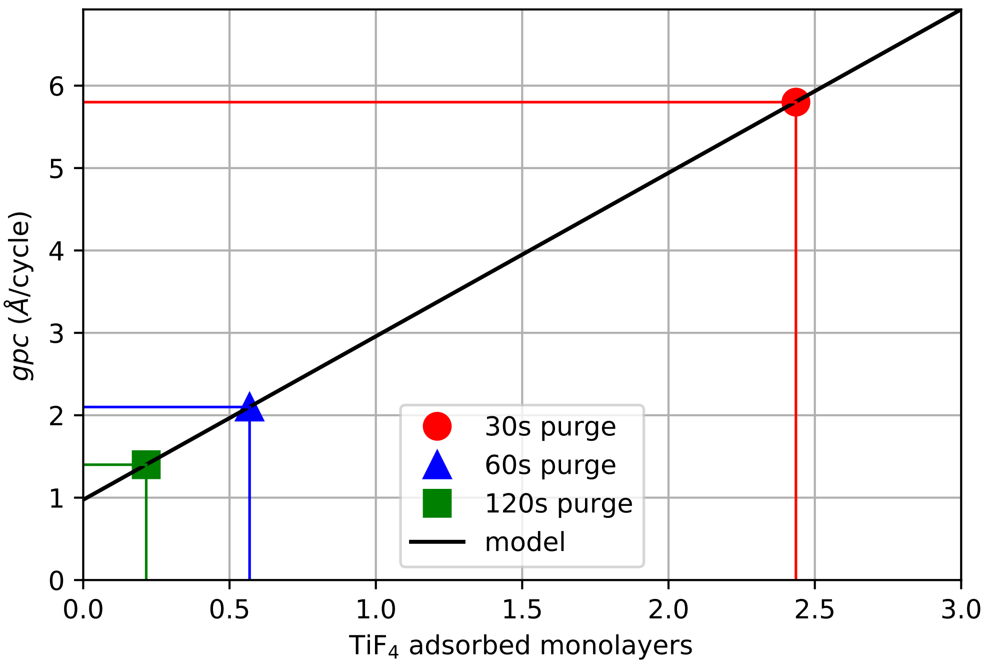

Figure 3.8: The predicted GPC as a function of the number of TiF_4 adsorbed layers n; experimentally determined GPC are indicated for runs D, E, and F.

with no over-saturation of TiF_4 and so GPC=1.15 Å. The decrease in measured GPC with increasing purge time is consistent with longer purge times leading to a greater degree of desorption of TiF_4(s).

Our deposition mechanism assumes the complete conversion of excess TiF_4 into AlF_3 during the TMA half-cycle with no Ti incorporation into the film. However, based on our film composition studies, we know this is not the case. To fully assess this, we note that further investigation may be needed for the role of incomplete conversion of adsorbed TiF_4 on GPC, e.g. $TiF_{4-y}(CH_3)_y$(b) for y $\in$ [0,4]. The study of TaF_5 from Jackson et al. had proposed a pathway of $TaF_{5-x}(CH_3)_x$ to further react and form TaC as a source of contamination.[36] Although C incorporation was found to be mostly adventitious, it is possible this a similar pathway in our system could generate C incorporation.

3.4.2 Impurity incorporation reactions

We examined the thermodynamic feasibility of a number of routes for potential oxygen incorporation in our films, such as whether the AlF_3 films can be directly oxidized and if residual TiF_4 incorporated in the film can be oxidized. The reactions considered are listed below; the Gibbs free energy values ΔG^o_{453} correspond to the reactor nominal operating temperature of 180° C.

Reaction			ΔG^o_{453} (kJ/mol)
$2AlF_3(s) + 3H_2O$	$\rightarrow$	$Al_2O_3 + 6HF$	256.8
$4AlF_3(s) + 3O_2$	$\rightarrow$	$2Al_2O_3 + 6F_2$	2493.6
$TiF_4(s) + O_2$	$\rightarrow$	$2F_2 + TiO_2$	641.4
$TiF_4(s) + 2H_2O$	$\rightarrow$	$4HF + TiO_2$	-18.7

We observe that:

1. AlF_3 is unreactive to H_2O and even less so with O_2, a result consistent with the findings of Mäntymäki et al. [5]

2. Residual TiF_4 is unreactive to O_2, but is reactive to H_2O with ΔG^o growing more favorable with increasing temperature, the latter observation that is consistent with high temperature TiO_2 ALD.[38] While there is no significant source of water within our reaction system while deposition takes place, exposing the hot wafer to lab atmosphere humidity after processing may account for some O incorporation.

3.5 Conclusion

AlF_3 films were grown by atomic layer deposition using TMA and TiF_4 as the precursor system. Initial deposition runs using this precursor system produced films composed of a 1:3.08 aluminum-to-fluorine atomic % ratio. Optically, AlF_3 films grown with undersaturated TiF_4 doses matched the expected refractive index value $n = 1.34$ (at 632.8 nm) cited in previous studies; however a steadily declining growth per cycle (GPC) with increasing number of cycles was observed and was attributed to a design flaw in our precursor delivery system. Subsequent runs corresponding to saturating doses of TiF_4 precursor generated films with surprisingly high GPC (>6 Å/cyc) accompanied by significant Ti incorporation. Although increased purge lengths after the TiF_4 exposure resulted in decreased Ti contamination, high O content was found in the films. A deposition model was developed based on these experimental observations using the double layer growth mode proposed by Mäntymäki et al., validating a plausible relationship between excess adsorbed TiF_4 and the higher than expected growth rates. Due to observed gradient formation and non-stoichiometric characteristics of films, further examination of this deposition process is continued in Chapter 4 for a more complete study of this AlF_3 ALD system.

Chapter 4: Investigation of tunable process parameters for optimization of aluminum fluoride ALD

4.1 Introduction

In ideal ALD, self-limited growth results from saturation of the growth surface by precursor ligands during one or more of the partial cycles. The growth per cycle (GPC) should be determined as a function of precursor dose and purge timings as illustrated in Figure 4.1. For a binary ALD process, the precursor exposure time, precursor purge time, co-reactant exposure time, and co-reactant purge time are tunable process parameters. GPC effect from each parameter are quantified by keeping three of the operating variables constant, while varying the fourth.[63] The overall effect of testing and optimizing these parameters is to confirm consistent self-limiting growth while generating a working recipe in which to operate the ALD process.

Ideally, a clear plateau of ALD GPC is observed when the GPC becomes insensitive to changes in the process operating conditions. For example, ALD can transition to chemical vapor deposition (CVD) when purge times are shortened to the point where the precursors interact in the gas phase or on the growth surface. Incomplete saturation due to lack of suitable exposure will reduce GPC and can cause unwanted thickness variation. In the case of industrial applications, it may also be important to note having too long a cycle will greatly increase fabrication time of thin films, especially for those requiring thousands of cycles.

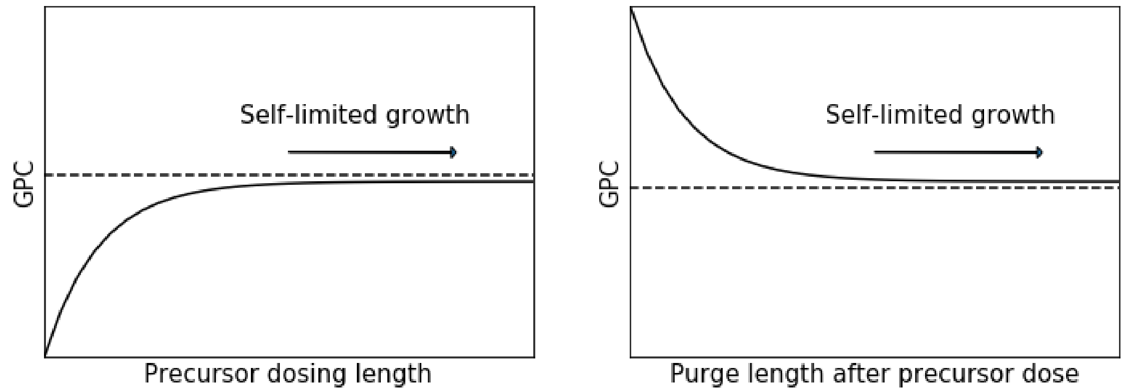

Figure 4.1: Ideal growth per cycle in ALD as a function of precursor dosing time (left) and purge time (right)

4.2 Second-generation AlF_3 ALD reactor design

The experiments in the previous chapter demonstrated successful ALD of aluminum fluoride films. Despite this success, the highly uncertain GPC along with the substanial Ti and O incorporation motivated an entirely new design for the reactor. A primary concern as the decrease in solid-state precursor sublimation pressure as cycle number increased. Likewise, spatial gradients in film thickness motivated a new reactor design. Meanwhile, experimentation with higher doses of titanium fluoride at a deposition temperature of 190°C led to a significant amount of titanium incorporated into film, resulting in undesirable optical properties.

These issues motivated new focus on TiF_4 precursor direct-dose management and new reactor design. This new reactor is outfitted with showerhead-type gas inlet designed to reduce gas-phase spatial gradient that can result in cross-flow reactors. Furthermore, a heated stage was included to promote uniformly heated substrates rather than reliance on conduction and convection from a heated wall design.

Experiments were designed to investigate whether we observe traditional self-limiting ALD behavior. Our hypothesis is as such – by tuning the two parameters of dosing and purge, we can influence the thickness and composition patterns of the thin films and compare the observed GPC to our model predictions. Thus, the following experiments were designed to confirmed our process objectively as an ALD process for generating self-limiting growth using the newly designed ALD reactor.

4.3 Materials and methods

4.3.1 Reactor Design

This study uses a custom-built hot-wall ALD shower-type reactor similar to design previously developed by NIST researchers.[64] A schematic diagram of the reactor system is presented in Figure 4.2 and a picture of the physical system is presented in Figure 4.3. The reactor chamber has a controllable gate valve which connects to two filters (Visi-Trap with SodaSorb and Posi-Trap with activated charcoal, Mass-Vac) and Edwards model RV5F mechanical vacuum pump which ultimately exhausts into a laboratory fume hood. MKS ALD pneumatic valves control precursor flow from the precursor bubbler (TMA) and sublimator (TiF_4) through a multi-input flange serving as an inlet to a conical diffuser above the sample stage. Argon purge gas feed is controlled with a mass flow controller (MKS P-series), set to a noncontinuous 10 sccm flow rate during experiments; the dynamics of noncontinuous purge flow are described in more detail later in this report. Direct sample stage heating is controlled through a dedicated stage heater (Blue Wave Semiconductors). The reactor body is heated using four thermostatically controlled ceramic heaters; other external components are heated using customized fitted jackets (MKS). A separate fitted MKS jacket is used to heat the TiF_4 sublimator. The TiF_4 input line is heated using a PID temperature controller to maintain a temperature gradient increasing from precursor source to reactor body to prevent TiF_4 condensation.

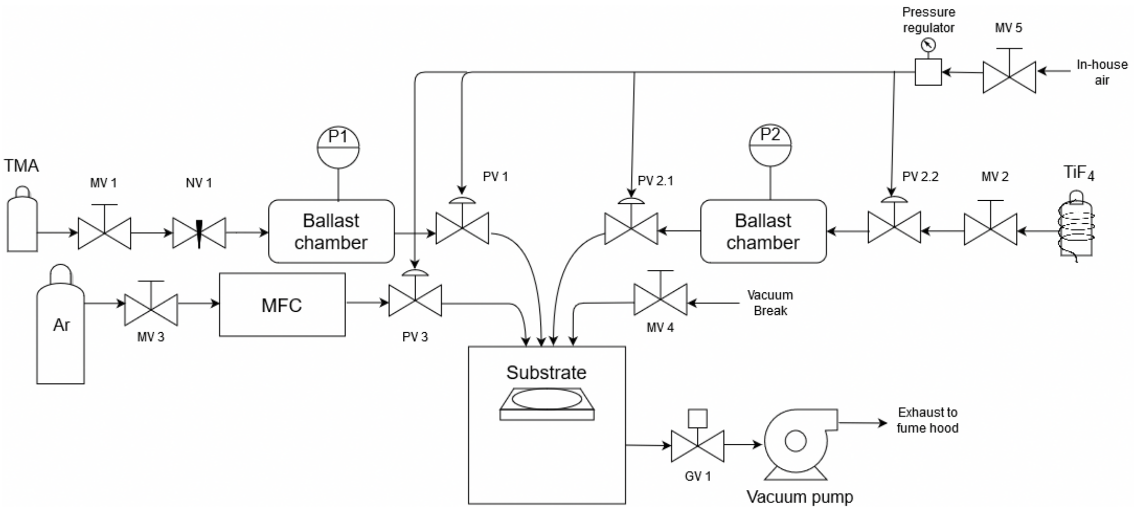

Figure 4.2: Schematic of next generation shower-type ALD reactor system.

Films from this process are deposited using TMA at room temperature and TiF_4 heated to 110°C. For optical application, it can be beneficial to deposit at lower temperatures as films are typically deposited as amorphous coatings with low roughness thereby reducing scattering of incident light.[34, 65] For AlF_3 ALD films, it was found that formation of crystalline structure began at deposition temperatures of 280°C, greatly increasing the roughness of the surface.[5] An additional concern when operating at higher temperatures are multiple reports of etching of AlF_3 films by TMA and HF precursor systems.[29, 33, 34] Therefore, the TiF_4 was set to 110 °C to generate an acceptable vapor pressure while deposition temperature was set at 150°C for this study to prevent potential condensation of the TiF_4 precursor.

Figure 4.3: Picture of shower-type ALD reactor system enclosed by heater jackets. Precursor and purge flow are controlled, entering from top of reactor and exhaust the bottom through a vacuum pump into the fume hood.

The ALD recipe design for a reactor system is defined by a combination of set operating conditions and timing sequences. Pulse and purge time sequences set for each precursor are defined for a single overall ALD cycle; the recipe repeats the timings for a specified number of ALD cycles. A simplified nominal timing sequence for our binary precursor system is denoted as t_1-t_2-t_3-t_4. For our system, t_1 refers to pulse time of TMA, t_2 purge time for reactor following the first pulse, t_3 the pulse time of TiF_4, and t_4 the subsequent purge time associated with TiF_4, all in seconds.

The overall dose-purge sequencing as seen in Figure 4.4 incorporates additional timing sequences for the direct draw system. Wait time (WT) specifies the condition of which all pneumatic valves are closed. Argon flow into reactor is designed to be only available during argon purge timing and is shut off at all other times. At the flow (10 sccm) of argon, the resulting reactor base pressures would greatly overwhelm the desired direct draw of TiF_4 precursor vapor pressure at 110°C. WT held prior to precursor doses allows reduction of reactor base pressure in the absence of argon, facilitating direct draw of TiF_4 low vapor pressure feed into the main body. As a further precaution for the direct draw precursor system, the WT immediately after precursor dose prevents argon from backflowing into feed lines. For this system, we found 5 and 1 seconds of purge to be necessary for reduction in base pressure prior to and after direct precursor draw, respectively. The cumulative purge time (with and without argon) is thus manipulated by adjusting the argon purge times while keeping all others constant, thereby enforcing a strict minimum of 6 seconds of purge time for the system. Lastly, for the TiF_4 precursor, opening of valve PV2.2 for 0.5 seconds draws vapor from sublimator into the TiF_4 ballast chamber, allowing TiF_4 vapor pressure to be confirmed directly before pulsing.

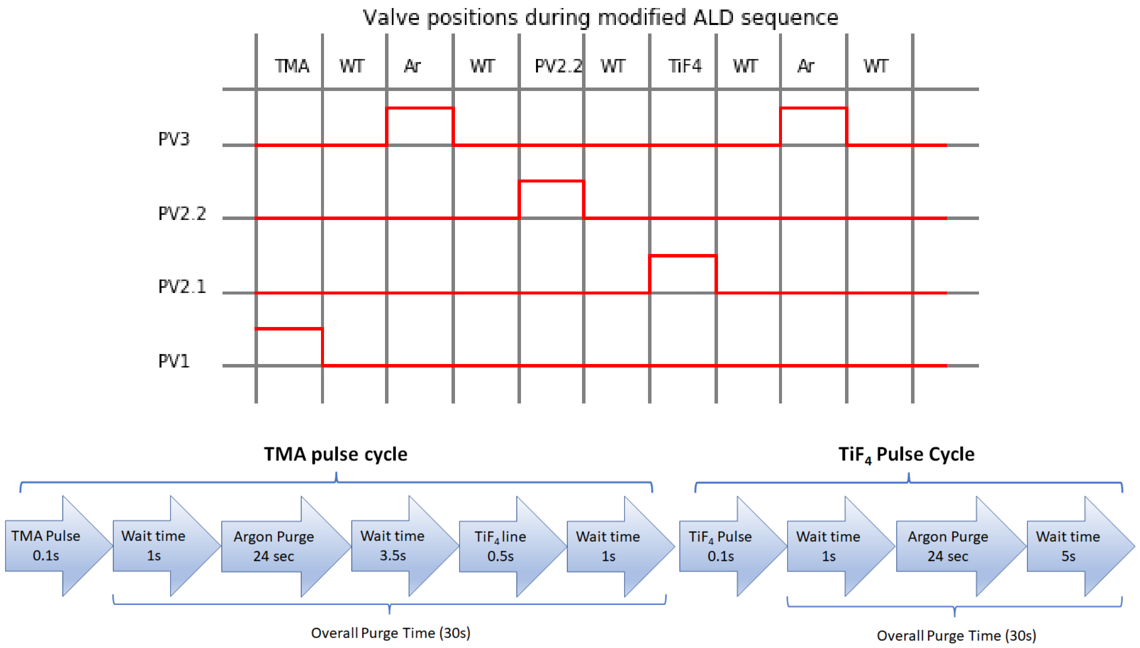

Figure 4.4: Sequence of operations for each ALD half cycle adjusted for direct draw of vapor pressure into reactor body (bottom). The vapor flow sequences (top) are controlled autonomously through four pneumatic valves, PV1, PV2.1, PV2.2, and PV3: PV1 opens TMA feed into reactor body, PV2.1 opens TiF_4 into reactor body, PV2.2 opens TiF_4 sublimator into the feed line, and PV3 opens argon into system. Wait times (WT) is incorporated to aide direct draw of precursors into reactor.

4.3.2 Experimental section

The substrates consist of single side polished Si(100) 2-inch wafers with ∼1.5 nm native oxide layer purchased from Virginia Semiconductor. Wafers were cleaned with ethanol in an ultrasonic bath for 5 minutes, rinsed with deionized water, and completely dried prior to deposition. TiF_4 (98%) was supplied from Strem Chemicals and TMA (97%) from Aldrich Chemistry. Ultra-high purity grade argon (99.999%) is used as purge gas and was supplied from Airgas. Reactor body and substrate sample stage were heated to 150°C. The TiF_4 sublimator was heated to a temperature of 110°C while TMA was maintained at room temperature. TiF_4 line was heated to 130°C, maintaining an increasing temperature gradient between sublimator and main body.

All film property measurements were conducted ex-situ. Optical measurements for thickness and refractive index were conducted using a J. A. Woollam M-2000D variable angle spectroscopic ellipsometer (VASE) at the University of Maryland NanoCenter at 65° and 70° angle settings. Film optical characterizations were generated using J. A. Woollam CompleteEASE software. Thickness and refractive index measurements were generated over 19 points in a hexagonal pattern about the wafer center. Samples were additionally measured by atomic force microscopy (AFM) on Bruker Dimension and Park-NX20 systems using tapping mode. A Hitachi SU-70 scanning electron microscope (SEM) with energy dispersive spectroscopy (EDS) also was used to confirm film composition.

4.4 Results and discussion

4.4.1 ALD film growth behavior

A series of films were deposited using the designed settings and recipes using 50 to 400 cycles. Using the timing sequence of 0.1-30-0.1-30 seconds, the films deposited exhibited an average GPC of 0.54 Å/cycle. Observed GPC values are slightly lower compared to those reported with the TMA/HF ALD precursor system (∼1.0 Å/cycle) deposited at 150°C.[29] Figure 4.5 shows an overall linear trend and low variance of thickness grown across many cycles with a linear fitting R^2 value of 0.987. A non-zero intercept is observed, a phenomena often seen in ALD due to

Element	5 keV Atomic %	15 keV Atomic %
F	57.2	67.2
Al	18.9	22.3
C	17.04	4.07
O	6.9	4.24

Table 4.1: Compositional analysis for AlF_3 film deposited with 200 ALD cycles using Hitachi SU-70 scanning electron microscope (SEM) with energy dispersive spectroscopy (EDS) at 5 and 15 keV accelerating voltage.

the difference of reactive Si substrate surface sites in early cycles to later reactive sites on the growing film.[66] Films were measured to have 1.38 refractive index on average at 632.8 nm. Alternative ALD precursor systems have reported similar low refractive indexes of ∼1.36 for this wavelength.[5, 9, 48]

A 200 cycle run using the 0.1-30-0.1-30 recipe was characterized with EDS confirming generation of AlF_3 composition and is summarized in Table 4.1. The ratio of Al:F is 1:3.03, showing relatively low oxygen counts. Carbon is also found to be present and is suspected to be adventitious as using a higher penetrating 15 keV stream showed a lower carbon content. The 4% of contamination amounts of C and O is comparable with other reported AlF_3 ALD studies, showing a significant improvement from the previous study in composition.[5, 29]

The wafers coated with [0, 50, 100, 150, and 400] ALD cycles were chosen for surface roughness characterization. In Figure 4.6, an overall baseline of 0.3 nm of measured rms roughness was found with the bare wafer over a 1x1 micron scanning area. After coating 50 and 100 cycles with deposition temperature of 150°C, the probed surface is featureless as expected of amorphous films. With confirmation of no significant roughness generation after deposition to surface, a larger scan size area

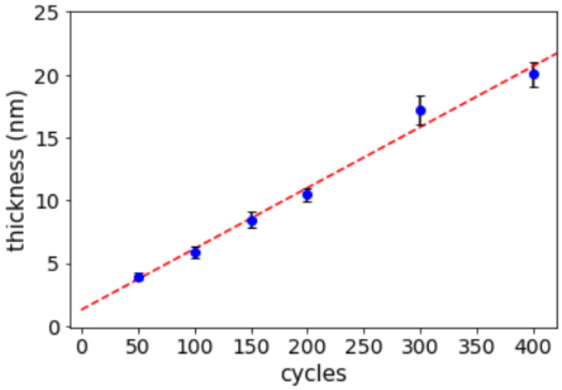

Figure 4.5: Observed thicknesses (nm) of ALD AlF_3 versus number of ALD cycles show consistent growth over 50 to 400 cycles with an average GPC of 0.54 Å/cycle. Error bars denote ± one standard deviation measured across 19 mapped points of wafer. Linear fitting generated a R^2 value of 0.987. A non-zero intercept (1.28 nm) is observed indicating a nucleation stage in early cycles.

Number of ALD Cycles	Film Thickness (nm)	Surface Roughness, rms (nm)
Bare Wafer	N/A	0.3
50	4.0	0.5
100	5.7	0.3
150	9.6	0.7
400	20.0	1.1

Table 4.2: Observed surface roughness (root mean squared) on AlF_3 deposited film thicknesses on Si substrates using AFM tapping mode. 0, 50, and 100 ALD cycles were measured by Park-NX20 system over a 1x1 micron scan area; 150 and 400 cycle samples which were measured by Bruker Dimension AFM over a 5x5 micron scan area

(5x5 micron) was investigated for uniformity of roughness for the subsequent 150 and 400 cycle samples. For the larger scan area the observed rms reaches maximum of 1.06 nm at 400 cycles. Thickness measurements and roughness characterization are summarized in Table 4.2. The low amount of roughness generated by this ALD process suggests minimal scattering impact as a transparent coating suitable for optical application extending into the far ultraviolet range.

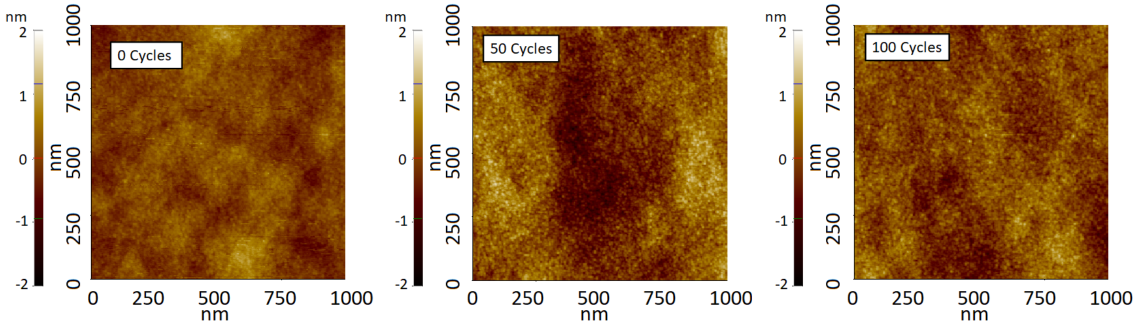

Figure 4.6: AFM topography images (1x1 micron scanning area) of polished Si wafer compared to 50 and 100 cycles of ALD AlF_3 found to be featureless i.e. amorphous when depositing at 150°C.

4.4.2 Self-limiting ALD growth

To further explain whether this AlF_3 ALD process is self-limiting, an additional set of experiments investigated the effect of adjustments to the 0.1-30-0.1-30 seconds ALD recipe. Parameters of the ALD process were tuned independently by changing either the number of precursor doses or precursor purge time length after each dose. To increase dosages, additional 0.1 second pulses of precursor were repeated up to 4 times separated by five seconds of wait time, effectively allowing further saturation by each precursor. The overall purge time lengths after doses were adjusted within the range from 6 to 120 seconds by increasing and decreasing the argon purge time length. Under these conditions, experiments were conducted to deposit AlF_3 films using 150 ALD cycles. The observed wafer-average GPC trends are summarized in Figure 4.7.

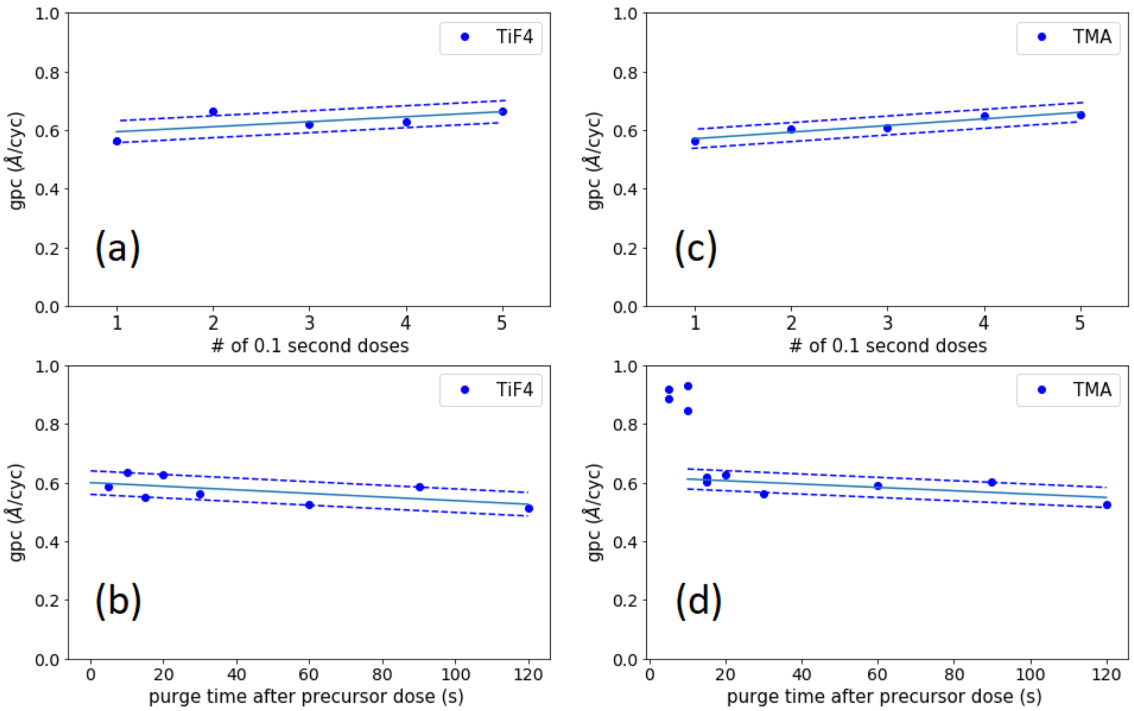

Figure 4.7: Average observed GPC across thickness mapped wafers are fitted to regressed lines with respect to changes in number of doses of precursor TiF_4 (a), purge length after TiF_4 exposure (b), number of doses of TMA (c), and purge length after TMA exposure (d) using 150 ALD cycles. Dashed lines refer to ± one standard deviation. Outliers are observed for purge times after TMA exposure lesser than 15 seconds for this reactor system and are omitted from regression analysis.

4.4.2.1 TiF_4 series

The average GPC resulting from increased TiF_4 doses is 0.62 Å/cycle, a slight increase from the standard recipe average GPC of 0.54 Å/cycle. A slight positive trend with slope of 0.017 Å/doses is seen in Figure 4.7(a). ALD systems with excess doses typically result in saturation of GPC, plateauing after a sufficient dose of precursor. The observed increase of GPC is likely indicative of absorption relative to precursor exposure onto reactor walls which slowly desorb during the ALD cycle to influence the GPC.[31] Nonetheless this effect remains relatively small as the

GPC among the 5 points of data falls within two standards of deviations. A R^2 value of 0.4 suggests weak correlation between the GPC and number of doses and that GPC is likely to have quickly plateaued for self-limiting growth with just one dose.

In Figure 4.7(b), a negative trend is observed corresponding to a slope of -0.0006 Å per seconds of purge after the TiF_4 dose. Increasing the purge length after the TiF_4 dose results in an average GPC of 0.57 Å/cycle. The phenomena of insufficient purge influencing higher GPC is unobserved in TiF_4 case and is most likely due to the controlled supply of TiF_4 vapor pressure at 110°C. The slowly decreasing trend while increasing purge length may be attributed to the slow desorption of adsorbed molecules from substrate surface during long purge times.[42] Nonetheless this decrease in GPC trend appears to remain relatively small; $R^2 = 0.37$ shows weak correlation between GPC and purge length. Similarly to dose, GPC is appears have quickly plateaued for self-limiting growth within the purge time range after 6 seconds.

4.4.2.2 TMA series

The average GPC from the including additional TMA doses in ALD recipe is 0.63 Å, slope showing a slight increase to 0.022 Å/doses. In Figure 4.7(c), a positive trend of 0.022 Å per TMA dose is observed with a much stronger fit ($R^2 = 0.93$) than that of TiF_4 dose and GPC. Here we note no effects from the earlier mentioned TMA etching reactions have been observed with increased TMA dose. As such, the linear increase of GPC with TMA dose is suspected to be similar in case to the TiF_4 doses in which increased wall adsorption effects on substrates as the increase is on the same order of magnitude. Higher correlation between GPC and TMA dose may be due to a significant difference in magnitude of vapor pressure of TMA having more consistent adsorption onto reactor walls for each additional pulse. Although there appears to be correlation between doses and GPC, the magnitude of GPC slope far from the originally measured 0.54 Å/cycle. Indication of subsaturation is not found between the 5 data points, and thus we believe one timed exposure of TMA to be sufficient for self-limiting growth.

Significantly higher GPC is found for purge times under 10 seconds or less, of up to 0.93 Å/cyc when using 10 seconds or lesser amounts of purge time length after TMA dose. In Figure 4.7(d), linear regression was performed for data points excluding outliers found higher than our predicted maximum GPC of 0.705. The high GPC observed at lower purge times is likely attributed to insufficient purge for the TMA precursor, depositing in a less controlled CVD-like growth mode instead. This phenomena is unobserved in TiF_4 case and is likely due to supply of relatively much lesser vapor pressure requiring less time to purge from the reactor system than TMA. At longer purge lengths of up to 2 minutes, we otherwise reach a minimal growth rate in both purge length cases. This effect is again attributed to slow desorption of adsorbed molecules from substrate surface during long purge times as the measured slope -0.00057 Å per second of purge after TMA dose is extremely similar. All data points fall within 2 standard deviations. A relatively weak correlation (R^2 = 0.38) for purge times and GPC while excluding outlier growths using 10 seconds or less of purge length after TMA dose. Because we do not see significant change after 15 seconds of purge time after TMA dose, we note the original 30 seconds to have been sufficient for self-limiting growth

4.5 Summary and Conclusions

The deposition of AlF_3 thin films by ALD was demonstrated using the novel precursor system of TMA and TiF_4 using our next-generation ALD reactor system. The earlier proposed reaction mechanism and model for this system predicts a theoretical GPC to be 0.705 Å per cycle. Deposition was conducted using a newly designed intricate timing sequence while making use of the ALD reactor's direct draw architecture. The films were measured for thickness via ex-situ multi-wavelength ellipsometry; amorphous ALD AlF_3 films were found to grow at roughly 0.54 Å per cycle at a deposition temperature of 150°C, producing films with refractive index of 1.38 at 632.8 nm. The investigation off exposure timings on GPC show that a single timed exposure for our system is sufficient for self-limited growth for both precursors. 6 seconds of purge after TiF_4 was found to be sufficient in removing gas phase byproducts due to controlled exposure, however purge timings require after TMA require at least 15 seconds of purge after TMA exposure to ensure self-limited growth free of gaseous byproducts and unreacted TMA.

Chapter 5: Space optical applications for aluminum fluoride ALD

5.1 Introduction

Astronomical observations in the Far ultraviolet (FUV) spectral region give insight to cosmic origin studies such as origin of large scale structures, the formation, evolution, and age of galaxies, and the origin of stellar and planetary systems.[24] Space optical instruments and telescopes, including NASA's flagship missions Hubble Space Telescope (HST) and Far-Ultraviolet Spectroscopic Explorer (FUSE), while working in the FUV region, face challenges of low resolution imaging. As one major constraint for these instruments and telescopes, mirror coatings have historically not performed well in the range, especially in the Lyman-α range of wavelengths (90-130 nm).[23] Investigators seek to enhance the working resolution of these instruments reflectivity over this wavelength range to increase the throughput of incident FUV wavelengths to sensors.

Aluminum mirrors are used in the Hubble Space Telescope (HST), protected by a thin coating of magnesium fluoride. While the reflectivity performance for HST has remained $> 80\%$ for wavelengths, $\lambda > 115$ nm, reflectivity dwindles to $<15\%$ for $\lambda \leq 110$ nm.[22] The more recent Far-Ultraviolet Spectroscopic Explorer (FUSE) used lithium fluoride coated aluminum mirrors and silicon carbide mirrors. Although the FUSE mission focused on far ultraviolet measurements, observations in the Lyman Ultraviolet Range (LUV, 91.2 - 121.6 nm) by Silicon Carbide (SiC) measured with a reflectivity of 40%, while Al+LiF, with a peak realized FUV reflectivity of 67% at 102.5 nm.[23] During operation it is further noted that there was significant degradation of reflectivity of the LiF coated mirror due to contact with humidity due to hygroscopicity of LiF.

Hourly rate of relative degradation of reflectivity per hour for unprotected LiF under 50% humidity has been reported by Fleming et al. (2017) in the form of two rates: 1.39 x 10^{-4} for $t < 350$ hr and 1.06 x 10^{-5} for $t > 600$ hrs, stating an overall degradation of 13.4% after 6 months.[22] The difference in order of magnitude of relative rate indicate that degradation rate under humidity will slow over time, and that LiF samples should be prioritized for low humidity storage staight after deposition. A recent report by Lewis et al. (2020) uses SEM to show LiF thin films to undergo irreversible changes when exposed to dew points greater than 6°C.[67] They suppose that a combination of deliquescence (physical uptake of water in LiF until forming a solution) and efflorescence (evaporation of water carrying LiF in solution) causes irreversible damage to the LiF optical properties and can be seen as a "blotchy" or hazy effect.

Metal fluorides have been traditionally used as transparent coatings on aluminum mirrors to prevent oxidization and that reduce the reflectivity of an Al surface. Additional thin film overcoats are being studied to further enhance passivation and maintain base reflectivity. Fleming et al. (2017) has reported LiF protection by ALD aluminum fluoride. The study makes use of the reaction between HF and TMA in Table 2.1 to coat Al+LiF mirrors fabricated by physical vapor deposition (PVD).[22, 26] While AlF_3 is a promising material as a transparent coating, Fleming et al. has noted that unlike LiF coatings, current AlF_3 coated Al mirrors only have suitable reflectivity for wavelengths above 106 nm, which limits observations at the Lyman-β range at 102.7 nm. As an advantage, AlF_3 is consider to be more resilient to humidity relative to LiF in preventing reduced reflectivity.[22] To overcome the barrier of maintaining reflectance at wavelengths corresponding to the lower Lyman range, Fleming et al. overcoated LiF+Al mirrors with 10-20 Å coating of ALD AlF_3 to have minimal impact on the reflectivity at $\sim$102 nm afforded by the thicker LiF layer while retaining higher resilience to humidity.

5.2 Motivation

In the previous chapters, the AlF_3 process that has been developed producees thin films with suitable refractive index and roughness as a ultraviolet transparent coating to have low effect on incident light. As the main goal of this study, we seek to confirm the suitability of our AlF_3 ALD process for reflectivity and performance in space optical applications similar to Fleming et al. In this case, performance is measured in terms of reflectance in the far ultraviolet but also to maintained reflectivity over time. In this chapter, we explore a collaborative effort with NASA-

Goddard Space Flight Center to coat Al-LiF mirrors with ALD AlF_3.

5.3 Material and Methods

The collaboration involves NASA-Goddard Space Flight Center's developmental PVD reactor system to physically deposit pure aluminum on a mirror blank followed by the deposition of a lithium fluoride (LiF). Deposition of Al and LiF layers onto two 2" single side polished Si(100) wafers fastened by large clips in this PVD system can seen in Figure 5.1. The process has been described in detail in an earlier reference.[11] Research later transitions into working with ultrasmooth 2" silica optical squares as substrates. Aluminum mirrors from NASA-Goddard Space Flight Center were coated with ∼65 nm of aluminum followed by ∼16 nm of LiF. Samples were then transferred to the AlF_3 ALD reactor at the University of Maryland to generate a thin AlF_3 overcoating layer. The AlF_3 coatings were generated with the nominal 0.1s-30s-0.1s-30s ALD sequencing recipe described in the previous chapter.

All far ultraviolet reflectivity of mirror samples were characterized by Dr. Luis Rodriguez de Marcos of NASA-Goddard Space Flight Center using a McPherson Vacuum Ultraviolet (VUV) 225 spectrophotometer. The spectrometer has a one-meter length high-vacuum monochromator with a 1200 lines/mm grating and operates at near-normal incidence in the spectral range from 30 nm to 325 nm. The spectrometer is equipped with a windowless hydrogen-purged light source, which provides discrete H emission lines between 90 nm and 160 nm and a continuum

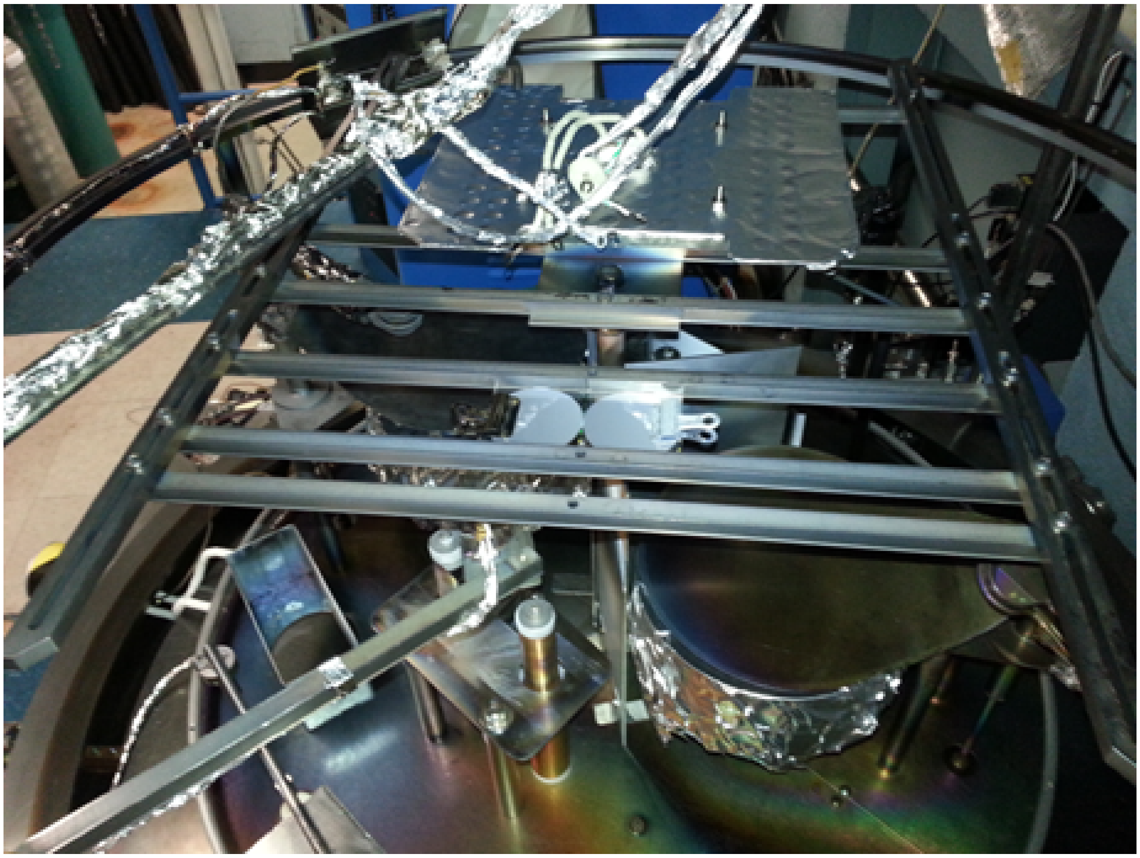

Figure 5.1: Silicon 2" wafer samples in the center held by large clips while being coated in the NASA-Goddard Space Flight Center PVD chamber awaiting to be deposited by a thick aluminum (∼65 nm) layer followed by a LiF coating (∼16 nm).

above these wavelengths. The detector consists of a photomultiplier cathode tube connected to a light-pipe for transferring the light signal out of the monochromator. The light pipe has a fluorescence and high quantum efficiency coating of sodium salicylate that is used to convert the FUV radiation into visible light. Absolute reflectance was obtained by alternately measuring the incident intensity and the intensity of the light beam reflected off the sample. Reflectance measurements were performed at 10° from normal incidence. Sample film thickness and refractive indices were characterized by J. A. Woollam M-2000D variable angle spectroscopic ellipsometer (VASE) at the University of Maryland NanoCenter at 65° and 70° an-

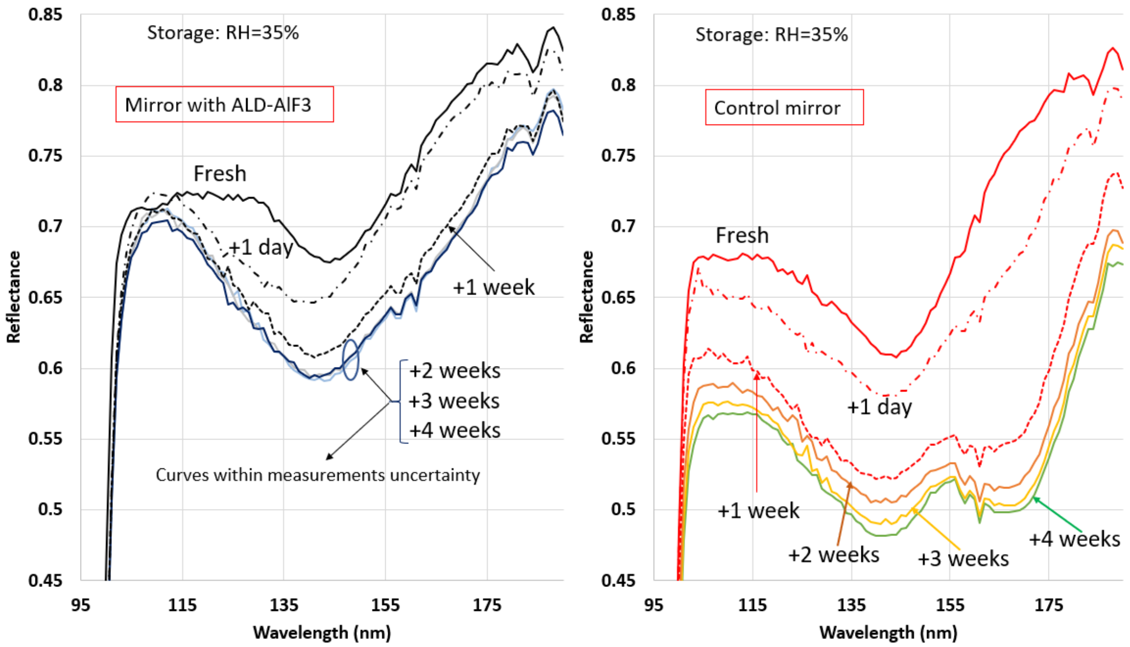

Figure 5.2: Noticeable improvement in maintained aluminum reflectance across 100-180 nm wavelengths over four weeks through overcoating of ALD AlF_3 coating: ALD AlF_3 overcoated aluminum mirror with LiF (left), aluminum mirror coated with lithium fluoride as control (right).

gle settings. Film optical characterizations were generated using J. A. Woollam CompleteEASE software. Two transparent Cauchy layers were modeled over bare Al to characterize the AlF_3 overcoating on Al-LiF mirrors.

5.4 Results

Twenty ALD cycles of the nominal 0.1s-30s-0.1s-30s AlF_3 recipe were conducted on one of the Si samples while the other was stored in dry box with 35% relative humidity as control. Because the AlF_3 ALD reactor did not require a fastener clip, AlF_3 is coated over both Al-LiF coated and uncoated regions on wafer. Ellipsometry after deposition confirmed a distinct small layer of ALD AlF_3 generated over the 16 nm LiF top layer. The AlF_3 was measured as 2.8 nm when characterizing both an uncoated and coated Al-LiF regions on the wafer. However, the exact thickness is still less certain due to the similarities of optical properties between LiF and AlF_3 and thinness of transparent AlF_3 layer. The LiF layer for the AlF_3 coated sample and control sample was measured to be 16.3 and 15.8 nm thick, respectively. Coatings were stored in a drybox with 35% relative humidity and reflectance was measured weekly over four weeks (Fig. 5.2). Overall the sample coated with AlF_3 was found to be more environmentally resilient, with an overall average of -8% reduction of reflectance on the overcoated sample versus -18.5% reduction in the control sample. Interestingly, degradation of LiF coated mirror can be visibly seen by the naked eye as soon as one week, as seen in Figure 5.3.

As seen in Figure 5.4, there is a sharp decline of reflectivity seen at wavelengths of interest (103 and 122 nm) within one day on both wafers. There remains a physical challenge of preventing exposure of sample to air while transporting of samples between the University of Maryland and NASA-Goddard Space Flight Center despite the relatively near locations. This highlights the time-sensitive exposure of LiF to air. In the study by Fleming et al. (2017), the researchers were able to circumvent this effect and maintain high reflectivity despite sending samples much farther distances (Maryland to California to Colorado) by holding samples in a dry N_2 environment between locations.[22] Despite the initial decrease of reflectivity, the sample overcoated by AlF_3 ALD maintains stable performance for the remainder of the four weeks as opposed to the control sample.

Following the success of this experiment, Al+LiF was deposited on a thick fused silica substrate (50x50x3.4 mm) and aged for two months. It is notable that

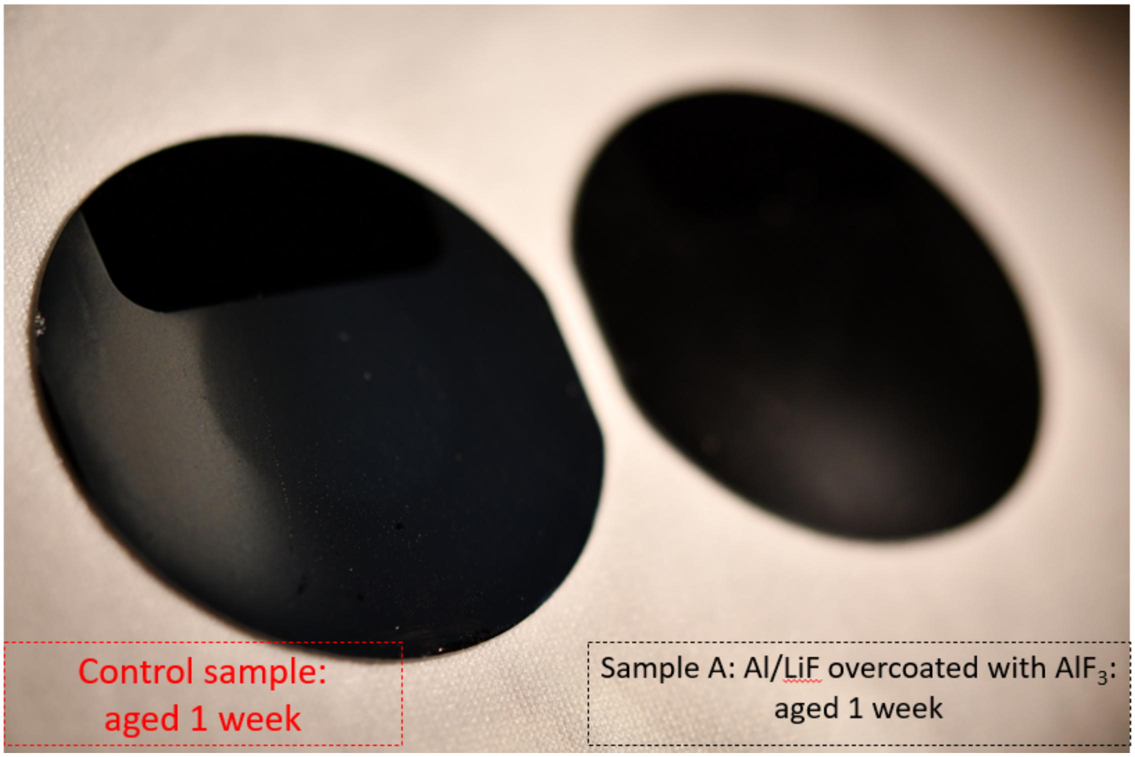

Figure 5.3: ALD AlF_3 overcoated aluminum mirror with LiF (right), aluminum mirror coated with lithium fluoride as control (left), both aged at 1 week. A slight circular haze in its center is noticeable for the control sample indicating some degradation of coating and is unseen in the AlF_3 overcoated sample. The top dark section on wafer lacks Al-LiF coating due to the large fastening clip used in PVD

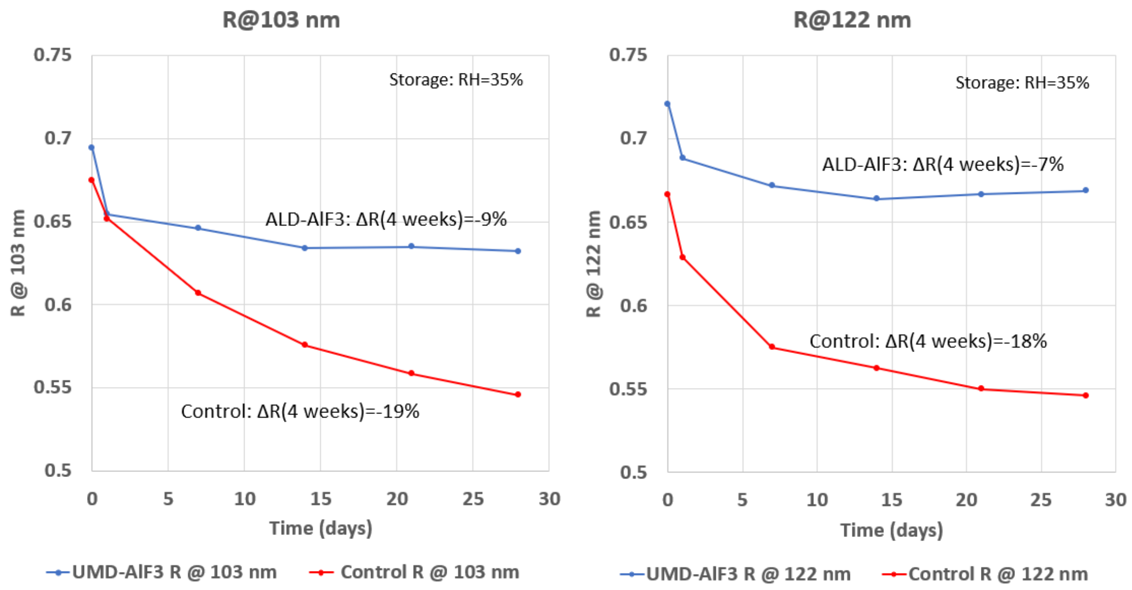

Figure 5.4: Comparisons of reflectivity performance between control and ALD overcoated mirrors at two wavelengths over four weeks (103 nm and 122 nm). While both samples show a sharp decline of reflectivity within the first day, the overcoated sample appears to mostly maintain reflectance values for the remainder of four weeks.

this glass substrate is intended for space optical applications rather than the previously used Si wafers. Reflectivity was measured before and after aging before overcoating the sample with AlF_3. 20 cycles of AlF_3 ALD were performed on the aluminum mirror coated with 16 nm of LiF. Ellipsometry characterization indicated a 1.4 nm thick ALD AlF_3 layer and a 16 nm thick layer of LiF. Reflectance measurements are presented in Fig. 5.5. Despite the similar profile of curves are seen in Fig. 5.5, the curves reveal several important features. First we note that the ALD process remains compatible with LiF mirrors while the LiF has partially degraded. Interestingly, the process improves reflectance for wavelengths above 107 nm. This is indicative of constructive interference despite change to the overall thickness for transparent layer and aging effects from the LiF+Al mirror. This phenomena is attributed to the differences in n and k values between LiF and AlF_3 at

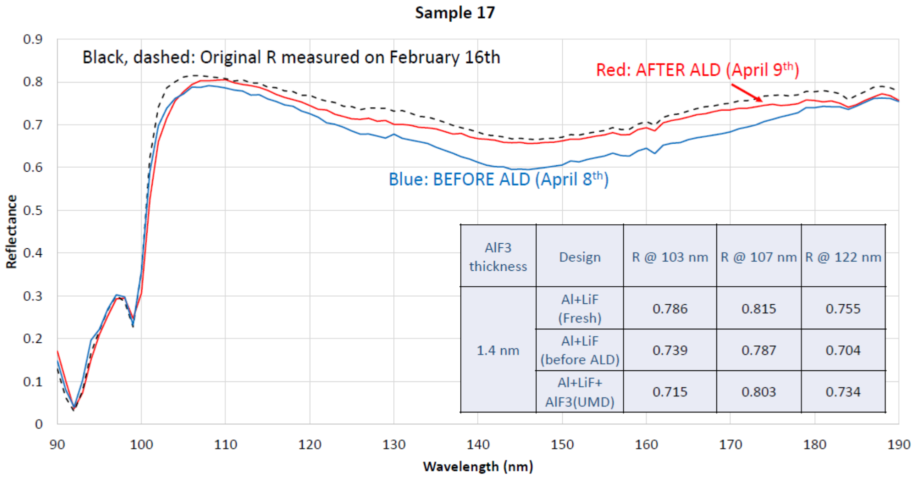

AlF3 thickness	Design	R @ 103 nm	R @ 107 nm	R @ 122 nm
1.4 nm	Al+LiF (Fresh)	0.786	0.815	0.755
	Al+LiF (before ALD)	0.739	0.787	0.704
	Al+LiF+ AlF3(UMD)	0.715	0.803	0.734

Figure 5.5: Minimal impact to overall reflective range found on space optical glass overcoated with AlF_3 ALD. The dashed black line indicates freshly deposited and measured Al-LiF sample, the solid blue line refers to measurements prior to transport to the University of Maryland, and the red line indicates measurement after AlF_3 overcoat.

each wavelength and of added thickness for optimal reflectivity.[22] Improvement of reflectance at higher wavelengths (>106.7 nm) is also reported by Fleming et al. (2017) for LiF+Al mirrors after treatment with AlF_3 ALD.

5.4.1 Cycle study on reflectance longevity

With the successful overcoating of AlF_3 on Al-LiF mirrors, further tests were conducted to study the effect of ALD cycles on the longevity of reflectance quality in the far ultraviolet. A sequence of ALD runs of [0, 10, 20, 50, 100, 200] cycles were performed on six Al-LiF mirrors using the AlF_3 ALD reactor with the goal of understanding the longevity of AlF_3 film performance as a function of film thickness. Surprisingly, thicknesses of AlF_3 characterized through ellipsometry do not follow the experimental GPC of 0.54 Å/cycle found last chapter as seen in Table 5.1. Specifically the AlF_3 does not show a linear trend in growth, as the 200 cycle run resulted in a thinner film relative to the 100 cycle run. While there may be difficulty in separating the two similarly optical layers of LiF and AlF_3, the combination of both layers also do not match up with in a linear pattern of thickness to cycle. A recent study from Hennessy et al. (2021) had also noted a similar interaction of low ALD growth on LiF samples albeit using a TMA/HF precursor system.[33] Hennessy et al. (2021) notes that having over 5 deposited pre-cycles of LiF ALD coating, will suppress AlF_3 growth. Despite using 500 cycles with this precursor system low growth of AlF_3 occurs regardless of deposition temperature whereas alternative aluminum sources TDMAA and DMAH paired with HF precusor readily grow AlF_3 on LiF. It was proposed in their study that there is a strong interaction between alkali halides and TMA to result in anomalous ALD growth. Briefly, it is suggested that after ligand exchange between LiF and TMA, $Li(CH_3)$ can re-interact with HF to reform LiF and compete with aluminum for the surface. Coupled with proposed AlF_3 etching reactions, this results in little AlF_3 remaining on surface. Although our system does not use HF as a precursor, a reaction pathway similar to this could account for the thickness anomalies found in Table 5.1. Future work will be to investigate this phenomena in detail.

Despite overall low AlF_3 growth observed on all samples, reflectance measurements remain prospective. Figure 5.6 shows a promising result with just 10 cycles of ALD overcoating, showing limited decrease in reflectance performance after 3 weeks. A preliminary assessment for all six samples after three weeks has found the reflectance at the Lyman-α wavelength of 121.6 nm to all have maintained 60% reflectance relative to the control sample without ALD overcoating. This set of

Sample	ALD cycles	Measured LiF thickness (nm)	Measured AlF_3 thickness (nm)
1	10	21.65	1.46
2	200	15.49	7.64
3	100	17.07	8.26
4	50	18.81	6.60
5	20	18.34	4.70
6	None	21.74	0

Table 5.1: Tabulated measured thicknesses for six lithium fluoride coated mirror samples overcoated using 0, 10, 20, 50, 100, and 200 cycles of nominal AlF_3 ALD recipe show anomalous ALD non-linear growth.

samples has been placed in a humidity chamber and far UV reflectance will be later assessed after a full year.

5.5 Concluding Remarks

Improvements in space optical devices for the far ultraviolet range require high transparency of incoming light to generate a high-quality image. AlF_3 ALD thin films generated from our process so far have demonstrated a suitable roughness, refractive index, and reproducible growth. Through collaboration with NASA-Goddad Space Flight Center, lithium fluoride coated aluminum mirrors were obtained as samples for testing the reflectivity performance in the FUV and robustness. Samples were measured for reflectivity using a McPherson Vacuum Ultraviolet 225 spectrophotometer. Using 20 ALD cycles to generate AlF_3 overcoat, initial Al-LiF mirrors deposited on Si wafers confirmed suitable transparency for Al-LiF mirror and excellent maintained reflectance in the far UV. After four weeks, reflectivity at the 103 nm wavelength decreased by 9% of base reflectance for the AlF_3 over coated sample, and 19% base reflectance for the control. Of the 9% reduced base reflectance,

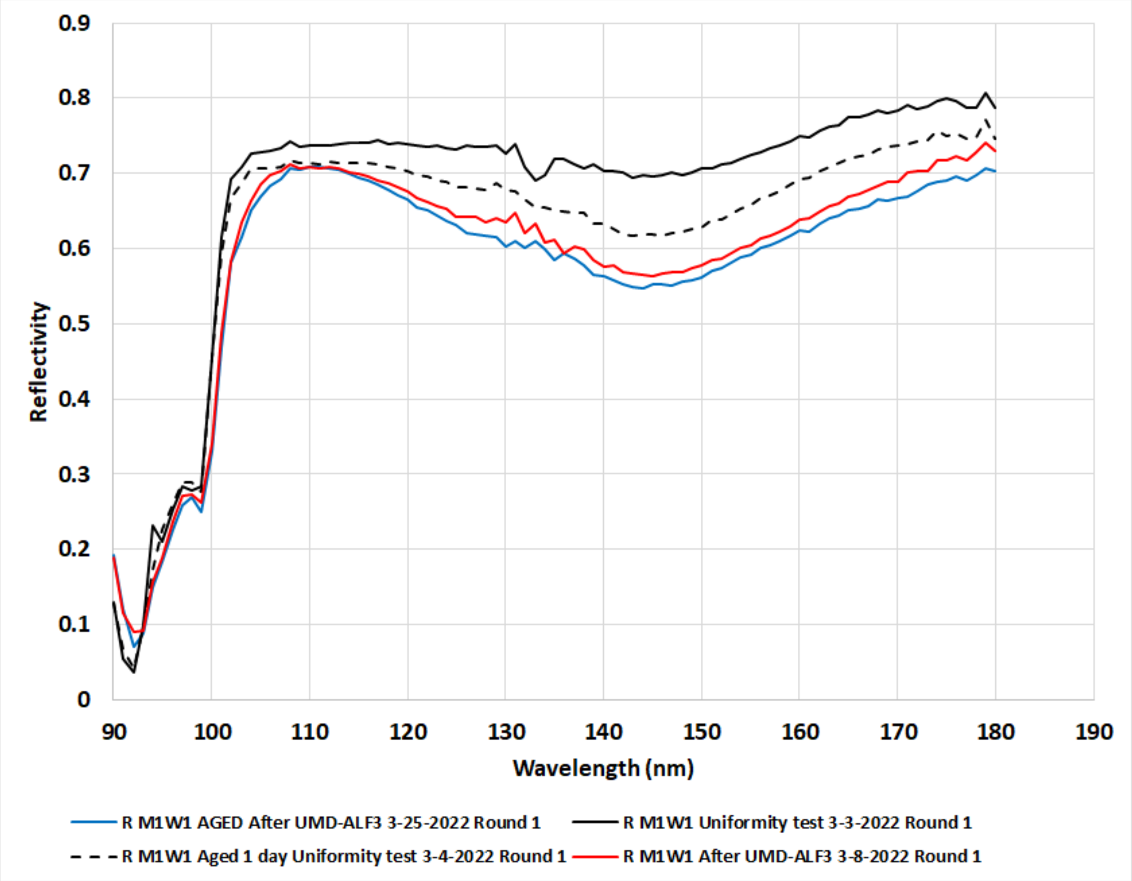

Figure 5.6: Far ultraviolet reflectance measured for fresh aluminum mirror coated with LiF (solid black), after one day (dashed black), after additional treatment of 10 ALD AlF_3 cycles (solid red), and after three weeks (solid blue). Reflectance after three weeks was found to maintain over 60% reflectance at the Lyman-α wavelength (121.6 nm) with low impact to overall reflectance.

the majority of degradation occurred on the first day during transport between NASA-Goddard Space Flight Center and the University of Maryland, largely due to the rapid degradation of LiF reflectivity. Space optic glass mirror samples coated by Al-LiF were confirmed to also have minimal impact to operable reflective range while maintaining good reflectivity over a month. The coating of six glass AlF_3 overcoated samples with a range of ALD cycles will be investigated over the course of a year to assess the overall longevity of these films.

Chapter 6: Conclusions and future works

6.1 Conclusions

The work presented in this thesis stems from the much larger NASA effort for developing broadband coatings for high performance mirror optics from infrared wavelengths down into the far ultraviolet spectral range. The developmental research described here has spanned from the investigation of thermochemistries expanding into a physically based ALD growth model for a novel two-precursor ALD system to the full design and engineering of two reactors for generating high-quality thin films as optical coatings. The first reactor, while successful at generating thin films with correct aluminum to fluorine stoichiometry and good refractive index, suffered from the undesirable qualities of film gradient formation, film impurities, and particle formation on the film surface stemming from the TiF4 precursor delivery. The current reactor has demonstrated reduced gradient formation through a design that reduces precursor flow asymmetries with a shower-head type configuration, using a simplified design subject to fewer sources of leaks, and with a modified design enabling consistent direct draw of TiF_4 vapor pressure operating at 110°C to fully eliminate particle formation. After establishing of self-limiting growth for this

ALD system, a collaboration between the University of Maryland AlF_3 ALD reactor and NASA-Goddard Space Flight Center Al/LiF physical vapor deposition reactor explored space optical applications for this metal fluoride thin film on aluminum mirrors.

Recalling the initial questions described in the introductory chapter:

- Will this ALD precursor system react to form AlF_3?

In chapter 2, we explore suitable ALD precursor systems for generating AlF_3 thin films, investigating trimethyl aluminum and titanium tetrafluoride precursors' suitability as ALD precursors. A reaction mechanism is proposed, describing each half-cycle ALD reaction step and consider the favorability for ligand exchange during the TiF_4 half cycle through bond energies. From here, a physically-based ALD model provides key insight on molecular-level surface species during saturating pulses and enables calculation of growth per ALD cycle.

- Is this process viable for ALD, i.e. are films able to be generated linearly with respect to thickness and reproducible under self-limiting growth?

Chapters 3 and 4 describe the ALD process development over the span of using two reactors. Using a cross flow-type reactor in Ch. 3, initial experiments highlighted the generation of AlF_3. XPS characterization showed a stoichiomery 1:3.08 Al:F ratio albeit indication of O, C, and Ti incorporation for multiple films. The found discrepancies in consistent growth per cycle and quality of film lead into new design of process and reactor in Ch. 4. Designing against the disadvantages encountered by the first reactor, the second reactor showed remarkable improvement in consistency of growth over many cycles of GPC $\simeq 0.6$ Å. Acceptable plateauing of GPC encountered while increasing dosage and purge timings show self-limiting ALD growth for the system.

- How do we qualify the quality of the film and will it be suitable for spacecraft application?

In Ch. 4, ALD AlF_3 thin films from our process was optically characterized with ellipsometry as a transparent film with a low refractive index of 1.38 at 632 nm wavelength. The film when measured by AFM showed a maximum of 1 nm of rough-mean-square roughness, indicating little to no scattering for far ultraviolet wavelengths of interest. Moving forward in Ch. 5, substrates shifted from Si bare wafers to physically deposited Al-LiF coatings on both wafers and optical glass. For spacecraft optical application, good quality metal fluoride coatings result in a minimal effect for the underlying material while passivating the material against deterioration effects from the environment. In this study, twenty AlF_3 ALD cycles were shown to greatly improve the resiliency of reflectivity in FUV wavelengths. Although reflectivity decreased after AlF_3 ALD overcoat, this effect was also observed in the uncoated Al-LiF mirror sample set as control and is attributed to the moisture-sensitive LiF layer. The thin ALD overcoat otherwise shows little to no change to underlying LiF and Al material for optical performance.

6.2 Future Work

6.2.1 AlF_3 ALD

The scope of this ALD work focused on generating samples suitable for space optics. Because of this, focus on low temperature deposition (150-200°C) was warranted as report of roughness above 220°C disallowed ellipsometry measurements due to high scattering of light.[5] As future work, a more complete profile of the appropriate temperature window for ALD will greatly enhance this ALD study, including higher temperatures to induce AlF_3 crystallinity. To study and confirm the proposed ALD reaction mechanism, additional in-situ characterization techniques (ellipsometry and mass spectrometry) are planned to be incorporated in reactor.

6.2.1.1 Principal component analysis

Over the course of this ALD work, a large number of wafers with spacially varying AlF_3 thicknesses and other quality characteristics have been fabricated. From ellipsometry, large data sets have gathered in the form of thickness maps and refractive indices which may be ideal for principal component analysis (PCA).[69] PCA aims to statistically reduce the dimensionality of the mapped 19 points across wafer followed by a reconstruction of the dataset. In performing PCA, we identify the dimensions which hold the most commonality between datasets.[70] In the context of thickness maps, we would expect to find a principal component with a directionally based pattern of which we may identify as specific to our reactor geometry. Conceptually by isolating a reactor profile pattern, other principal components could then be isolated as process parameter patterns.

Preliminary work for this uses the mapped wafers in the thickness-cycle dataset in Sect.4.4.1 to draw out 19 paired eigenvalue-eigenfunctions from a covariance calculation before reordering pairs from highest to lowest eigenvalues. Reconstruction of data indicates three out of the nineteen principal components are sufficient to regenerate the GPC profile on wafer as seen in Fig. 6.1. Furthermore, analysis for this particular dataset show that over 95% of the variance may be explained through PC1 alone. Intuitively for this dataset it may be plausible to characterize these functions as related to reactor geometry, number of ALD cycles, and experimental error. Future work using this methodology would include forming a more heuristic approach to identifying key principal components in the context of ALD data and process parameters. Formalization of this technique may help aide diagnosis of ALD ideal growth patterns by being able to identify and isolate anomalous growth patterns.

6.2.2 Aluminum mirror coatings

One of the main challenges of working with aluminum mirrors is the need for passivation of surface prior to transport with the readiness to oxidize. As such, LiF was physically deposited over on Al mirrors prior to transport from NASA-Goddard Space Flight Center to the University of Maryland. Future work on Al mirrors would ideally involve keeping samples in vacuum by making reactors all in-house or forming a transportation strategy for samples similar to Fleming et al. (2017). Furthermore, although this study focused on FUV reflectivity performance, future work may include a wider band of spectrum to characterize for a more detailed study. As an additional note, LiF's hygroscopicity has been noted several times to case deterioration of reflectivity however the study of the exact interactions with moisture may be useful in future experiments.

6.2.2.1 UVO cleaning

Ultraviolet ozone (UVO) cleaning is a standard process typically used for cleaning items such as wafers, AFM probes, and metal surfaces.[68] Intuitively the use of ozone for fluoride samples is a bit strange as ozone has the potential to act as an energetic oxygen source potentially able to interact with the fluoride film. Use of UVO on an AlF_3 overcoated LiF+Al mirror sample show very promising results as seen in Figure 6.2. This sample was cleaned for 20 mins and at 70°C using UVO. Despite the initial concern of O incorporation, reflectance measurements in the FUV revert to initial reflectance values similar to those seen while freshly coated despite being over five months old. It is suspected that the successful reversion of the reflectance degradation indicates that a superficial layer of carbon and other organics are able to be safely removed by UVO for the AlF_3 coated LiF mirror and that the mirror is resilient to O incorporation. While more testing is needed, UVO may serve as a useful tool in future fluoride mirror coatings as a way to combat degradation during operation.

6.2.2.2 XeF_2 treated Al mirror samples

Alternative from LiF passivation of samples, Quijada et al. (2021) also describes a potential XeF_2 treatment for physically deposited Al mirrors to form a very thin layer on the order of a few nanometers of AlF_3.[11] Preliminary tests seek to combine this XeF_2 technique to generate a temporary thin AlF_3 cap before being transported to the ALD reactor at the University of Maryland to be grown to a larger thickness for reflectivity measurements. Current efforts so far have not been successful at generating a mirror with reflectance profile characteristic of pure AlF_3 over Al through this process. It is suspected that the passivated layer formed from XeF_2 is not stable enough for transport between the two facilities or that a fundamental chemistry after XeF_2 treatment prevents correct generation of AlF_3 growth. Future work seeks to identify the fundamental cause for this through characterization and analysis of these samples.

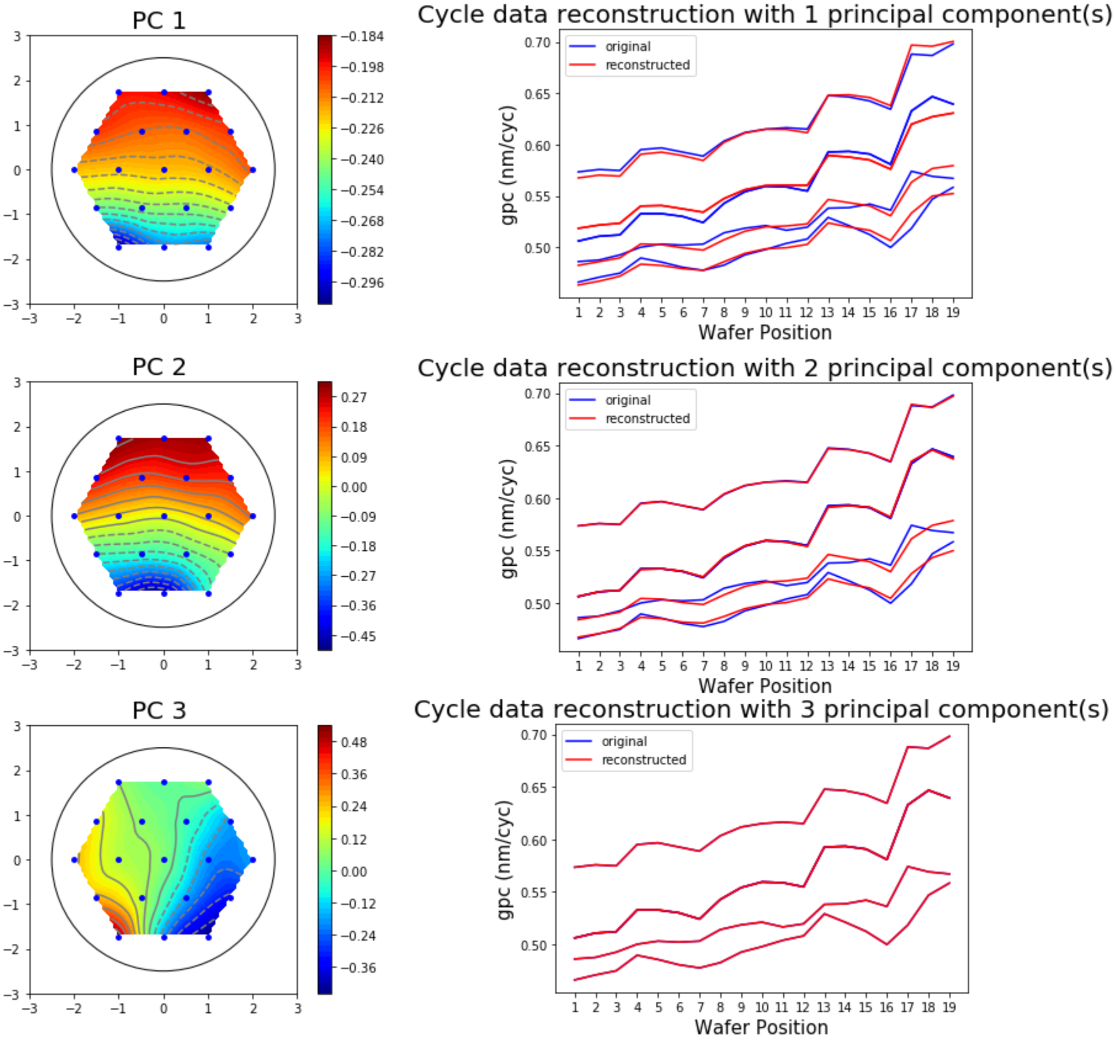

Figure 6.1: Principal component analysis performed using 19 point mapped wafer from Sect.4.4.1 showing the highest scoring principal components PC1, PC2, and PC3's profile and regeneration of the wafer maps by those three eigenfunctions alone.

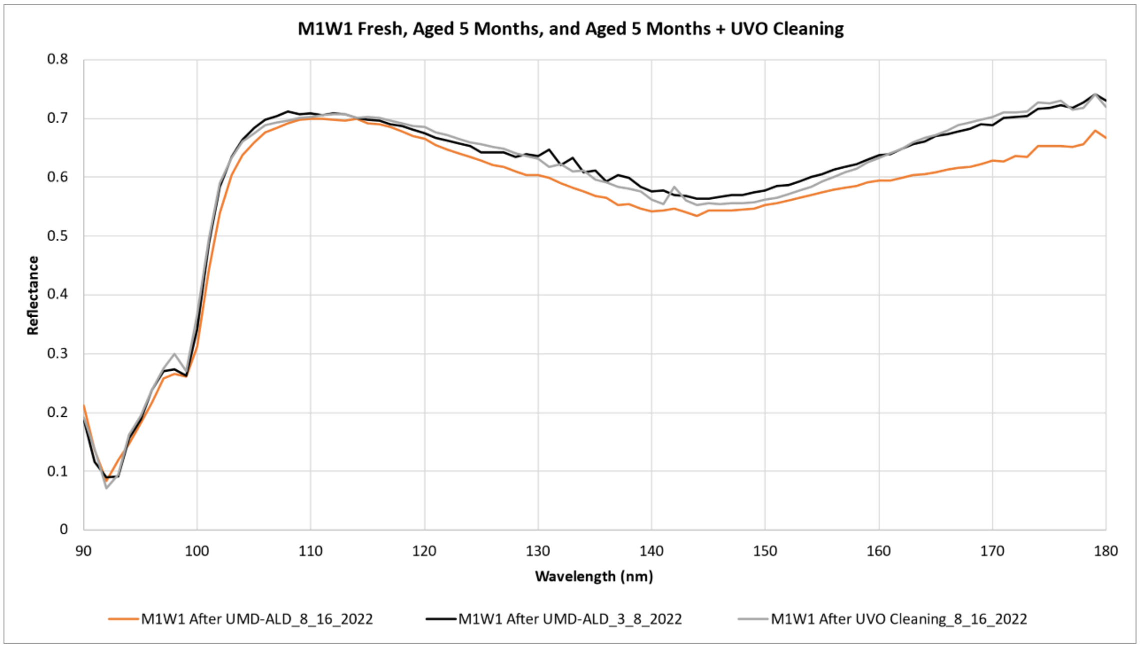

Figure 6.2: LiF performance is restored through UVO cleaning to initially measured reflectance values. The black curve is the reflectance measured after deposition, the orange line is reflectance measured after aging 5 months, and the gray line is reflectance measurement of the aged sample after UVO cleaning.

Bibliography

[1] Adomaitis, R. , Development of a multiscale model for an atomic layer deposition process. *J. Cryst. Growth* 312(8), 1449-1452 (2010).

[2] Adomaitis, R. Dynamic order reduction of thin-film deposition kinetics models: A reaction factorization approach. *Journal Of Vacuum Science & Technology A*. **34**, 01A104 (2016)

[3] Mansoori, G. & Soelaiman, T. Nanotechnology - An Introduction for the Standards Community. *Journal Of ASTM International*. **2** pp. 1-21 (2005,6).

[4] Krahl, T., & Kemnitz, E. Aluminium fluoride - the strongest solid Lewis acid: Structure and reactivity. *Catalysis Science & Technology*, 7(4), 773-796. (2017).

[5] Mäntymäki, M., Heikkilä, M. J., Puukilainen, E., Mizohata, K., Marchand, B., Räisänen, J., ... Leskelä, M. Atomic Layer Deposition of AlF3 Thin Films Using Halide Precursors. *Chemistry of Materials*, 27(2), 604-611. (2015).

[6] Riello, D., Zetterström, C., Parr, C., Braulio, M., Moreira, M., Gallo, J., & Pandolfelli, V. AlF_3 reaction mechanism and its influence on α-Al_2O_3 mineralization. *Ceramics International*, 42(8), 9804-9814. (2016).

[7] Gutierrez-Luna, N., Perea, B., Espinosa-Yanez, L., Honrado-Benitez, C., Lis, T., Marcos, L., Aznarez, J. & Larruquert, J. Temperature Dependence of AlF_3 Protection on Far-UV Al Mirrors. *Coatings*. **9** pp. 428 (2019,7)

[8] Brillson, L. J. (2016). An Essential Guide to Electronic Material Surfaces and Interfaces.

[9] Vos, M. F., Knoops, H. C., Synowicki, R. A., Kessels, W. M., & Mackus, A. J. (2017). Atomic layer deposition of aluminum fluoride using Al(CH3)3 and SF6 plasma. *Applied Physics Letters*, 111(11), 113105.

[10] George, S. Atomic Layer Deposition: An Overview. *Chemical Reviews.* **110**, 111-131 (2010).

[11] Quijada, M., Hoyo, J., Gray, E., Richardson, J., Howe, A., Marcos, L. & Sheikh, D. Influence of evaporation rate and chamber pressure on the FUV reflectance and physical characteristics of aluminum films. *UV/Optical/IR Space Telescopes And Instruments: Innovative Technologies And Concepts X.* **11819** pp. 118190G (2021)

[12] H.C.M. Knoops, S.E. Potts, A.A. Bol, and W.M.M. Kessels, Ch. 27 - Atomic Layer Deposition (pp. 11011134) in Handbook of Crystal Growth, edited by T. Kuech (Elsevier, 2015).

[13] Hwang, C. Atomic layer deposition for semiconductors. Springer, New York (2014).

[14] Gakis, G., Vergnes, H., Scheid, E., Vahlas, C., Caussat, B. & Boudouvis, A. Computational Fluid Dynamics simulation of the ALD of alumina from TMA and H2O in a commercial reactor. *Chemical Engineering Research And Design.* **132** pp. 795-811 (2018).

[15] Kumar, A., Singh, R. & Bahuguna, G. Thin Film Coating through Sol-Gel Technique. *Research Journal Of Chemical Sciences.* **6** pp. 65 (2016,6).

[16] Vossen, J., Kern, W. & Kern, W. Thin Film Processes II. Academic Press (1991).

[17] Biyikli, N. & Haider, A. Atomic layer deposition: an enabling technology for the growth of functional nanoscale semiconductors. *Semiconductor Science And Technology.* **32**, 093002 (2017,8).

[18] Puurunen, R. A Short History of Atomic Layer Deposition: Tuomo Suntola's Atomic Layer Epitaxy. *Chemical Vapor Deposition.* **20**, 332-344 (2014) .

[19] Miikkulainen, V., Leskelä, M., Ritala, M. & Puurunen, R. Crystallinity of inorganic films grown by atomic layer deposition: Overview and general trends. *Journal Of Applied Physics.* **113**, 021301 (2013).

[20] Salami, H. (2019). *An experimental and graph theoretic study of atomic layer deposition processes for spacecraft applications.* [Doctoral dissertation, University of Maryland, College Park]. ProQuest Dissertations Publishing.

[21] Moore, C., Hennessy, J., Jewell, A., Nikzad, S. & France, K. Recent developments and results of new ultraviolet reflective mirror coatings. *Space Telescopes And Instrumentation 2014: Ultraviolet To Gamma Ray.* **9144** pp. 91444H (2014).

[22] Fleming, B., Quijada, M., Hennessy, J., Egan, A., Hoyo, J. D., Hicks, B. A., . . . France, K. Advanced environmentally resistant lithium fluoride mirror coatings for the next generation of broadband space observatories. *Applied Optics*, 56(36), 9941. (2017).

[23] Quijada, M. A., Walton, S. G., Boris, D. R., & Hoyo, J. G. Improved mirror coatings for use in the Lyman Ultraviolet to enhance astronomical instrument capabilities. UV/Optical/IR Space Telescopes and Instruments: Innovative Technologies and Concepts VIII (2017).

[24] Salumbides, E. J., Bagdonaite, J., Abgrall, H., Roueff, E., & Ubachs, W. H2 Lyman and Werner band lines and their sensitivity for a variation of the protonelectron mass ratio in the gravitational potential of white dwarfs. Monthly Notices of the Royal Astronomical Society, 450(2), 1237-1245 (2015).

[25] France, K. C., Harris, W. M., Fleming, B. T., West, G. J., Mccandliss, S. R., Omeara, J., ... Pascucci, I. The LUVOIR Ultraviolet Multi-Object Spectrograph (LUMOS): Instrument definition and design. UV, X-Ray, and Gamma-Ray Space Instrumentation for Astronomy XX. (2017).

[26] Hennessy, J., Balasubramanian, K., Moore, C. S., Jewell, A. D., Nikzad, S., France, K., & Quijada, M. Performance and prospects of far ultraviolet aluminum mirrors protected by atomic layer deposition. *Journal of Astronomical Telescopes*, Instruments, and Systems, 2(4), 041206 (2016).

[27] Lee, C., Liao, B. & Liu, M. Developing new manufacturing methods for the improvement of AlF3 thin films. *Opt. Express.* **16**, 6904-6909 (2008,5).

[28] König, D., Scholz, R., Zahn, D. R., & Ebest, G. Band diagram of the AlF3SiO2Si system. *Journal of Applied Physics*, 97(9), 093707 (2005).

[29] Lee, Y., Dumont, J. W., Cavanagh, A. S., & George, S. M. Atomic Layer Deposition of AlF3Using Trimethylaluminum and Hydrogen Fluoride. *The Journal of Physical Chemistry C*, 119(25), 14185-14194 (2015).

[30] Balasubramanian, K., Hennessy, J., Raouf, N., Nikzad, S., Ayala, M., Shaklan, S., ... Quijada, M. Aluminum mirror coatings for UVOIR telescope optics including the far UV. UV/Optical/IR Space Telescopes and Instruments: Innovative Technologies and Concepts VII (2015).

[31] Salami, H., Poissant, A., & Adomaitis, R. A. Anomalously high alumina atomic layer deposition growth per cycle during trimethylaluminum under-dosing conditions. *Journal of Vacuum Science & Technology A* 35(1) (2017).

[32] Salami, H., Uy, A., Vadapalli, A., Grob, C., Dwivedi, V., & Adomaitis, R. A. Atomic layer deposition of ultrathin indium oxide and indium tin oxide films using a trimethylindium, tetrakis(dimethylamino)tin, and ozone precursor system. *Journal of Vacuum Science & Technology A*, 37(1), 010905 (2019).

[33] Hennessy, J., Jewell, A., Jones, J.P., Crouch, G., & Nikzad, S. Aluminum Precursor Interactions with Alkali Compounds in Thermal Atomic Layer Etching and Deposition Processes. *ACS Applied Materials & Interfaces*, 13(3), 4723-4730 (2021).

[34] Messina, D., Eller, B., Scowen, P., & Nemanich, R. Comparison of AlF_3 thin films grown by thermal and plasma enhanced atomic layer deposition. Journal of Vacuum Science & Technology A, 40(1), 012404 (2022).

[35] Pilvi, T., Ritala, M., Leskelä, M., Bischoff, M., Kaiser, U., & Kaiser, N. Atomic layer deposition process with TiF_4 as a precursor for depositing metal fluoride thin films. *Applied Optics*, 47(13) (2008).

[36] Jackson, D. H., Laskar, M. R., Fang, S., Xu, S., Ellis, R. G., Li, X., ... Kuech, T. F. Optimizing AlF3 atomic layer deposition using trimethylaluminum and TaF_5: Application to high voltage Li-ion battery cathodes. *Journal of Vacuum Science & Technology A*, 34(3), 031503 (2016).

[37] Dumont, J. W., & George, S. M. Competition between Al_2O_3 atomic layer etching and AlF_3 atomic layer deposition using sequential exposures of trimethylaluminum and hydrogen fluoride. *The Journal of Chemical Physics*, 146(5), 052819 (2017).

[38] Pore, V., Kivelä, T., Ritala, M., & Leskelä, M. Atomic layer deposition of photocatalytic TiO_2 thin films from TiF_4 and H_2O. *Dalton Transactions*, (45), 6467 (2008).

[39] Nieminen, H.E., & Ritala, M. Reaction mechanism studies on atomic layer deposition process of AlF_3. *Journal of Vacuum Science & Technology A*, 40(2), 022401 (2022).

[40] Dean, J. Lange's Handbook of Chemistry. McGraw-Hill, (1992).

[41] Travis, C. D., & Adomaitis, R. A. Modeling ALD Surface Reaction and Process Dynamics using Absolute Reaction Rate Theory. *Chemical Vapor Deposition*, 19(1-3), 4-14 (2013).

[42] Puurunen, R. Growth Per Cycle in Atomic Layer Deposition: Real Application Examples of a Theoretical Model. *Chemical Vapor Deposition.* **9** pp. 327 - 332 (2003,12).

[43] Blumenfeld, R. Disorder Criterion and Explicit Solution for the Disc Random Packing Problem. *Phys. Rev. Lett.*. **127**, 118002 (2021,9).

[44] Mondello, M., Grest, G., Webb, E. & Peczak, P. Dynamics of n-alkanes: Comparison to Rouse model. *The Journal Of Chemical Physics.* **109**, 798-805 (1998).

[45] Roodenko, K., Halls, M. D., Gogte, Y., Seitz, O., Veyan, J., & Chabal, Y. J. Nature of Hydrophilic Aluminum Fluoride and Oxyaluminum Fluoride Surfaces Resulting from XeF2 Treatment of Al and Al2O3. *The Journal of Physical Chemistry C*, 115(43), 21351-21357 (2011).

[46] Weckman, T., & Laasonen, K. Atomic Layer Deposition of Zinc Oxide: Diethyl Zinc Reactions and Surface Saturation from First-Principles. *The Journal of Physical Chemistry C*, 120(38), 21460-21471 (2016).

[47] Ohlidal, I. & Navratil, K. Method for determining the refractive index and thickness of a non-absorbing thin film with randomly rough boundaries. *Thin Solid Films.* **44**, 313-321 (1977).

[48] Hennessy, J., Jewell, A. D., Balasubramanian, K., & Nikzad, S. Ultraviolet optical properties of aluminum fluoride thin films deposited by atomic layer deposition. *Journal of Vacuum Science & Technology A*, 34(1) (2016).

[49] Banks, B. A., Groh, K. K., & Miller, S. K. Low Earth Orbital Atomic Oxygen Interactions with Spacecraft Materials. MRS Proceedings, 851 (2004).

[50] NIST Chemistry WebBook, SRD 69. (n.d.). Retrieved from https://webbook.nist.gov/chemistry/

[51] Webb, S. & Gordon, M. Intermolecular Self-Interactions of the Titanium Tetrahalides TiX4 (X = F, Cl, Br). *Journal Of The American Chemical Society.* **121**, 2552-2560 (1999).

[52] Hall, E. H., Blocher, J. M., & Campbell, I. E. Vapor Pressure of Titanium Tetrafluoride. *Journal of The Electrochemical Society*, 105(5), 275 (1958).

[53] Hess, A., Kemnitz, E., Lippitz, A., Unger, W. & Menz, D. ESCA, XRD, and IR Characterization of Aluminum Oxide, Hydroxyfluoride, and Fluoride Surfaces in Correlation with Their Catalytic Activity in Heterogeneous Halogen Exchange Reactions. *Journal Of Catalysis.* **148**, 270 - 280 (1994).

[54] Liao, B., Hsiao, C. & Lee, C. Aluminum oxyfluoride films for deep ultraviolet optics deposited by a combined HIPIMS/CFUBMS deposition technique. *Optical Materials Express.* **6** pp. 1506 (2016,5).

[55] Auciello, O. Science and technology of thin films and interfacial layers in ferroelectric and high-dielectric constant heterostructures and application to devices. *Journal Of Applied Physics.* **100** pp. 051614-051614 (2006,9)

[56] Mousty-Desbuquoit, C., Riga, J. & Verbist, J. Electronic structure of titanium(III) and titanium(IV) halides studied by solid-phase x-ray photoelectron spectroscopy. *Inorganic Chemistry.* **26**, 1212-1217 (1987).

[57] Groner, M., Fabreguette, F., Elam, J. & George, S. Low-Temperature Al2O3 Atomic Layer Deposition. *Chemistry Of Materials.* **16**, 639-645 (2004).

[58] Huang, Y., Pandraud, G. & Sarro, P. Characterization of low temperature deposited atomic layer deposition TiO2 for MEMS applications. *Journal Of Vacuum Science & Technology A.* **31**, 01A148 (2013).

[59] Pliskin, W. A., & Esch, R. P. Refractive Index of SiO_2 Films Grown on Silicon. *Journal of Applied Physics*, 36(6), 2011-2013. (1965).

[60] Li, J. & Talu, O. Effect of Structural Heterogeneity on Multicomponent Adsorption: Benzene and p-Xylene Mixture on Silicalite. *Fundamentals Of Adsorption.* **80** pp. 373 - 380 (1993).

[61] Fukazawa, Y., Miyazaki, K., Sanpei, K., Nakajima, T., & Takase, K. The Influence Of Native Oxide On Si Wafer Cleaning. International Symposium on Semiconductor Manufacturing, Extended Abstracts of ISSM (1994).

[62] Titanium(IV) fluoride; MSDS No. 333239 [Online]; Sigma-Aldrich: St. Louis, MO, May 27, 2016. https://www.sigmaaldrich.com/catalog/product/aldrich/333239 (accessed Nov 10, 2018).

[63] M.F.J. Vos, A.J.M. Mackus, W.M.M. Kessels. Atomic Layer Deposition Process Development 10 steps to successfully develop, optimize and characterize ALD recipes. AtomicLimits. (2019, 3).

[64] Kimes, W., Moore, E., & Maslar, J. Perpendicular-flow, single-wafer atomic layer deposition reactor chamber design for use with in situ diagnostics. *Review of Scientific Instruments*, 83(8), 083106. (2012).

[65] Quijada, M. A., Boris, D. R., del Hoyo, J., Wollack, E. J., Kozen, A. C., Walton, S., & Dwivedi, V. E-beam generated plasma etching for developing high-reflectance mirrors for far-ultraviolet astronomical instrument applications. Space Telescopes and Instrumentation 2018: Ultraviolet to Gamma Ray, 10699, 728738 (2018).

[66] Puurunen, R. Surface chemistry of atomic layer deposition: A case study for the trimethylaluminum/water process. *Journal Of Applied Physics.* **97**, 121301 (2005).

[67] Lewis, D., Plewe, C., Stapley, A., Vawdrey, J., Turley, R. & Allred, D. Illuminating the degradation of lithium fluoride mirror coatings in humid environments. *Advances In Optical And Mechanical Technologies For Telescopes And Instrumentation IV.* **11451** pp. 1145141 (2020)

[68] Vig, J. UV/ozone cleaning of surfaces. *Journal Of Vacuum Science & Technology A.* **3**, 1027-1034 (1985).

[69] Adomaitis, R. A reduced-basis discretization method for chemical vapor deposition reactor simulation. *Mathematical And Computer Modelling*. **38**, 159-175 (2003).

[70] Shlens, J. A Tutorial on Principal Component Analysis. *Educational*. **51** (2014,4).

Publications and conference presentations

Publications

[1] Salami, H., Uy, A., Vadapalli, A., Grob, C., Dwivedi, V. H., & Adomaitis, R. A. Atomic layer deposition of ultrathin indium oxide and indium tin oxide films using a trimethylindium, tetrakis(dimethylamino)tin, and ozone precursor system. *Journal of Vacuum Science & Technology A*, 37(1), 010905 (2019).

[2] DeCarlo, S., & Uy, A. Still Afloat? A Look at the Helium Industry. Executive Briefings on Trade. United States International Trade Commission, Office of Industries. (2017).

[3] Uy, A. Systems engineering-based model development: Application to predictive simulation of a net-zero home. Masters Thesis, University of Maryland, College Park. (2017). https://search.proquest.com/docview/1959336426?accountid=14696

Publication to be submitted:

[4] Uy, A., Dwivedi, V. H., Rodriguez de Marcos, L., Quijada, M., & Adomaitis, R. A. An Atomic Layer Deposition Process for Aluminum Fluoride Thin Films Using Trimethyl Aluminum and Titanium Tetrafluoride as Precursors, (tentative submission 2022).

Conference Presentations

[1] Dwivedi, V. H., Adomaitis, R. A., Salami, H., Uy, A., Vadapalli, A., Sheard, B., & Degroh, H. Growth and Modification of Carbon Nanotubes By Atomic Layer Deposition of Ni and Cu for Spaceflight Instruments and Terrestrial Applications. Paper presented at 2019 AIChE Annual Meeting, Orlando, FL (2019).

[2] Adomaitis, R. A., Salami, H., Uy, A., Vadapalli, A., Sheard, B., & Dwivedi, V. H. Growth and Modification of Carbon Nanotubes By Atomic Layer Deposition of Ni and Cu for Spaceflight Instruments and Terrestrial Applications. Paper presented at 2019 AIChE Annual Meeting, Orlando, FL (2019).

[3] Uy, A., Salami, H., Vadapalli, A., Grob, C., Dwivedi, V. H., & Adomaitis, R. A. Atomic layer deposition of aluminum fluoride for use in optical devices. Paper presented at AVS 19th International Conference on Atomic Layer Deposition, Bellevue, WA (2019).

[4] Salami, H., Uy, A., Dwivedi, V. H., & Adomaitis, R. A. Investigation of Electrical and Optical Properties of Indium Oxide Thin-Films Prepared By Atomic Layer Deposition Using Trimethylindium and Ozone Precursors. Paper presented at 2018 AIChE Annual Meeting, Pittsburgh, PA (2018).

[5] Uy, A. & Adomaitis, R. A. Physically Based Dynamic Modeling for Predictive Simulation of a Net-Zero Home. Poster presented at 2018 AIChE Annual Meeting, Pittsburgh, PA (2018).

[6] Dwivedi, V. H., Hasegawa, M., Adomaitis, R. A., Salami, H. & Uy, A. Modification of Radiator Pigments by Atomic Layer Deposition (ALD). Paper presented at the 48th International Conference on Environmental Systems ICES-2018-16, Albuquerque, NM (2018).